How can Deteriorated Concrete Half-Joint Structures be Assessed?

by

Richard Jenkins (EM)

Fourth-year undergraduate project in
Group D, 2014/2015

I hereby declare that, except where specifically indicated, the work submitted herein is my own original work.

Signed: ____________________________ Date: ______________

Technical Abstract

How Can Deteriorated Concrete Half-Joint Structures be Assessed?

Richard Jenkins (EM), Group D

A half-joint bridge is a type of reinforced concrete structure that was popular during the 1960s and 70s. It consists of a central span that is lifted into place and is characterised by the joint between two dapped end beams. Concern has been raised about this type of structure, as many fail assessments to current standards. This was heightened by the collapse of the De La Concorde overpass in Quebec, Canada in 2006. The Commission of Inquiry [Johnson et al., 2007] into this collapse suggested a possible cause may have been corrosion around the reinforcement anchorage region near supports. This report presents a series of experiments designed to help in understanding the effect of this corrosion on the concrete-steel bond.

This work focuses specifically on cracks that are formed along the reinforcement in the concrete. These cracks are formed by the expansive pressure that arises because the products of corrosion occupy a greater volume than the reactants. Isolating this effect should enable a greater understanding of the effect of cracks on bond to be formed, which could offer significant benefits in the analysis and assessment of existing half-joint structures.

In order to investigate this, a series of eccentric pull-out tests were performed. These consisted of a 305mm high, 200mm wide, 300mm long concrete block with four ϕ10mm reinforcement bars placed at 46mm cover in each corner. These reinforcement bars were then pulled out using a hydraulic jack. This test method was chosen as it is a more accurate representation of beam behaviour than a cylindrical pull-out test and allows the testing of multiple reinforcement. It was also simpler to produce than full beam tests, allowing a greater number of tests to be performed.

Two approaches were used to place cracks in samples. Firstly, embedded precracked cylinders were used. These consist of 100mm diameter concrete cylinders, which are cast with reinforcement passing through, cracked using a splitting apparatus and then embedded into the final sample block. Artificial cracks were also produced, using either a sheet of cling-film or aluminium foil to simulate the crack, or alternatively by performing a multi-stage cast with debonding oil applied at the interfaces.

Failure by both pull-out and splitting mechanisms was observed during testing. Uncracked datum samples failed in pull-out at an average ultimate bond strength in the range 15.9MPa to 17.0MPa. It was shown that a crack can have a significant impact on bond strength. Our experiments showed that a 30mm crack radius gave a negligible 3% decrease in ultimate bond strength, whilst a crack to the surface of the test specimen (radius of 50mm) reduced ultimate bond strength by approximately 40%, failing in pull-out. Splitting failure was shown to be determined by the amount of confinement, itself related

to the length of crack along the bar. Samples with a crack radius of 50mm and length of 100mm generally failed in pull-out at an average ultimate bond strength of 10.6MPa, however splitting occurred in one sample at 12.5MPa. Placing the crack across the whole length of the sample (300mm) caused a splitting failure to occur at a considerably reduced average ultimate bond strength of between 3.3 and 6.0MPa for the different methods of artificial crack production. Cracked samples were shown to experience a stress-slip relationship similar to uncracked samples, exhibiting a slip at ultimate bond of between 1&2mm, as suggested by the FIB Model Code 2010 [FIB, 2012].

Aluminium Foil was discounted as a method of artificial crack production due to it reacting with the concrete. Oil was discounted due to a large variation in results, owing to the difficulty in ensuring that an equal amount of oil was applied to the interface. Samples utilising plastic cling-film are shown to behave similarly to precracked cylinders, thereby providing a simple method for placing cracks into future test specimens.

A significant "Top Bar Effect" was observed, whereby top cast bars have between 50-72% lower ultimate bond strength than bottom cast bars. This is considerably higher than the 30% decrease suggested by Eurocode 2 [British Standards Institution, 2010]. It is thought this is the result of plastic settlement due both to insufficient curing and the leakage of cement paste through formwork after casting.

The failure mechanism is shown to have a significant effect on both the residual bond and strength of adjacent bars. Samples failing in pull-out had a residual bond strength after failure equal to approximately 43% of ultimate strength, whereas those failing in splitting could only sustain 25% of their ultimate strength. Pull-out failure, being a localised failure of concrete, has little or no effect on the bond strength of adjacent bars, whereas splitting failure is shown to cause a significant (~47%) reduction in the ultimate bond strength of adjacent bars.

It is shown that design codes are very conservative - Eurocode 2 gives a design bond strength of 1.74MPa for our test specimens. As such, it is thought that the code, albeit not explicitly, makes some allowance for these cracks along the bar. An approach to predicting ultimate bond strength is presented, based on an extension to work by Tepfers [1973]. It is suggested that additional experiments could be performed in order to develop empirical equations relating crack and confinement characteristics to the ultimate bond strength due to pull-out and splitting failure modes. These equations would give the Engineer confidence to assume that cracked samples can sustain full design bond strength, allowing assessments to take account of the significant bond that can still be developed when cracks are observed along the reinforcement due to corrosion.

Contents

Thanks

The author wishes to thank Dr Janet Lees & Dr Pieter Desnerck for their assistance and support during this project, as well as Martin, Dave, Luke, Jan & Phil in the Structures Laboratory for their assistance and advice regarding the experimental aspects of the project.

Word Count

This report consists of 11,926 words.

List of notation

Symbol	Represents	Units
α	Bond angle (See Figure 2.1)	Degrees
$\sigma_{\theta\theta}$	Tangential stress	MPa (N/mm^2)
σ_{rr}	Radial stress	MPa (N/mm^2)
τ	Bond stress	MPa (N/mm^2)
τ_{max}	ultimate bond strength	MPa (N/mm^2)
$\tau_{u,split}$	Bond Strength at Splitting Failure - FIB [2012]	MPa (N/mm^2)
τ_f	Residual Bond strength - FIB [2012]	MPa (N/mm^2)
ϕ	Reinforcement bar diameter	mm
c	Cover from bar to surface	mm
e	Radius of cracking	mm
f_c	Compressive Cylinder strength of concrete	MPa (N/mm^2)
f_{cu}	Cube compressive strength of concrete	MPa (N/mm^2)
f_{ck}	Characteristic value of cylinder compressive strength of concrete	MPa (N/mm^2)
f_{ct}	Tensile strength of concrete	MPa (N/mm^2)
h_r	Height of ribs on reinforcement	mm
l_e	Bond length	mm
r	Distance (radial)	mm
s_r	Spacing of ribs on reinforcement	mm
s	Slip	mm
s_1	Slip at start of ultimate bond strength plateau - FIB [2012]	mm
s_2	Slip at end of ultimate bond strength plateau - FIB [2012]	mm
s_3	Slip at Residual Bond Strength FIB [2012]	mm

1 Introduction and aims

1.1 Half-Joint Bridges

A Half-Joint Bridge is a category of reinforced concrete bridge that was widely used during the motorway construction boom in the 1960s and 1970s. The method is characterised by the joint detail between two dapped-end beams, as shown in Figure 1.1. It became popular as a result of its simple lift-in construction and there are currently over 300 such structures under Highways England's management [Highways Agency, 2004]. Concern has recently been expressed over the continued safe operation of these structures (many of which fail an assessment according to current standards), particularly regarding chloride-rich water ingress which leads to corrosion in and around the half-joint.

The concern over these bridges and desire to better understand their behaviour was heightened by the collapse of the De La Concorde Overpass in Quebec, Canada in 2006. This bridge collapsed under normal load conditions, causing the loss of five lives. The Commission of Enquiry [Johnson et al., 2007] into the collapse listed a number of "principal reasons" for the bridge's failure: poor detailing and installation of reinforcing bars as well as poor quality concrete in the abutments played a significant role in the collapse. A further "principal reason" was the poor anchorage of reinforcement in regions away from the half-joint. The ability for bond to develop between concrete and steel reinforcement plays an important role in allowing a bridge to develop full capacity. Corrosion was observed to be present in the bond anchorage region in the De La Concorde Bridge. This report investigates the effect of this corrosion on bond.

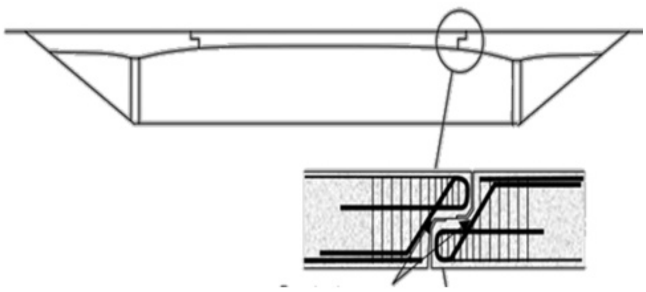

Figure 1.1: Half Joint bridge: Typical detail - Highways Agency [2004]

1.2 Corrosion & Bond

The most common approach to modelling the effect of corrosion on concrete is to use an accelerated corrosion method, whereby the reinforcement is connected to an electrical current and placed in a solution to artificially accelerate the corrosion process, such as in Fang et al. [2004] (Figure 1.2). However, the current research project will build upon work being undertaken into an alternative approach, whereby the effects of corrosion are

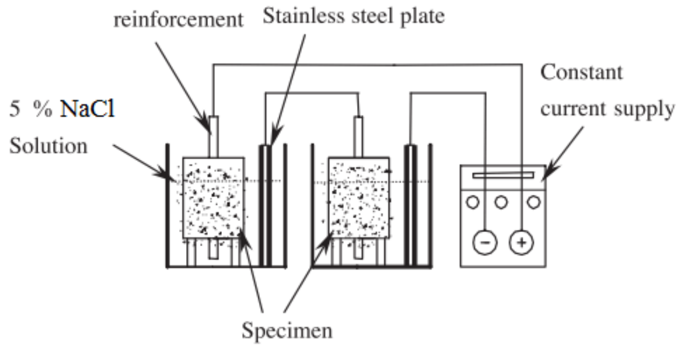

Figure 1.2: Accelerated Corrosion Process - from Fang et al. [2004]

modelled directly. [Desnerck et al., 2015]

There are three main effects of corrosion: (i) the products of the corrosion reaction occupy a greater volume than the reactants, causing an increase in the effective diameter of the bar. Lundgren [2007] has shown that this increase in volume can give a small increase in bond strength initially, before the bond is significantly weakened by the cracking of the surrounding concrete caused by the expansive pressure that arises because of this volume increase. (ii) These products cause a weak layer to form around the bar, giving an effective smoothing of the bars. Mangat and Elgarf [1999] have shown that this can cause an increase in the slip (movement) between reinforcement and concrete. (iii) The reduction in cross-sectional area of the reinforcement due to the corrosion gives a decreased tensile capacity.

This research will concentrate on these cracks in the surrounding concrete, isolating this effect in order to better understand the impact it has on bond behaviour. Concrete samples with cracks adjacent to the bond will be created and bond strength tested in order to find an experimental link between crack formation and bond characteristics. In order to achieve this, an alternative testing method that allows the testing of multiple reinforcement bars in a setup simulating half joints will be used. Simultaneously, different methods of casting concrete samples with cracks will be investigated, and the resulting method used to compare behaviour of the cracked and uncracked bond behaviour. It is hoped that this work will eventually make possible accurate assessments of the strength of bond in regions of corrosion, as current practice is conservative, with bond being taken either as full strength (uncracked), or zero (cracked). In addition, it is thought this method could offer advantages to bridge assessors, as cracks are observable and easily measured, whereas measurement of corrosion in concrete is often impractical, as the methods available, such as corrosion potential measurements are often both destructive and expensive.

Part I

Theory & Previous work

2 Theory of Bond

The bond between concrete and steel is a fundamental part of the behaviour of reinforced concrete structures. The mechanics of this bond mechanism have been studied in detail, most notably by Tepfers [1973]. In this section, an overview of the mechanisms involved in the concrete-steel bond will be given. This will initially deal with uncracked samples, as is covered by existing work. Suggested modifications to include pre-existing cracks in the concrete will be made in Section 8.

2.1 A theoretical explanation of bond

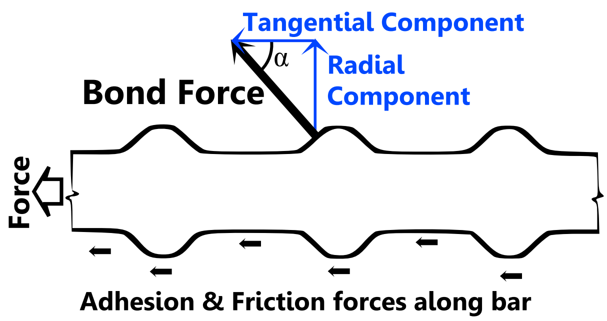

Figure 2.1: Components of Bond - Adapted from Darwin and Matamoros [2003]

Tepfers [1973] suggests that the bond exerts a bearing force acting at an angle α to the bars. This leads to a stress with components both radial and tangential to the bars. Whilst the tangential force provides the bond strength, it is the radial force that controls failure. Tepfers idealises this force as a uniform pressure acting on a thick walled concrete cylinder. In addition to this bearing force, Darwin and Matamoros [2003], amongst others, suggest the two other components of bond as adhesion and friction (Figure 2.1). The stages of bond behaviour can be described in four stages corresponding to increasing load. First, there is an initial phase whereby friction and adhesion exist such that a load can be carried with very little slip. In this phase, Tepfers suggests that the concrete surrounding the bond behaves elastically. Secondly, radial cracks begin to occur as a result of the internal pressure; however the partially-cracked concrete can still carry a significant additional force. Thirdly, failure occurs. This can be a pull-out failure, where bearing stresses cause localised concrete crushing as well as a shear plane to form around the bar, or splitting failure, whereby the radial stresses fail the surrounding concrete in tension. Finally, after failure, bond stress decreases whilst slip increases until a residual strength is reached, beyond which stress is constant for increasing slip. These stages will be evaluated and a series of bounds produced on loads at different stages.

2.1.1 Initial stage

Adhesion, caused by chemical action and aggregate interlock, will alongside friction, provide an initial resistance to slip of the bond. However, this is generally small. According to Tepfers, the component of the bond perpendicular to the bar can be taken as an internal pressure in a thick walled concrete cylinder. Equilibrium analysis on the setup in Figure 2.2a leads to the formation of an equation for equilibrium.

$$\sigma_{\theta\theta} - \sigma_{rr} - r\frac{d\sigma_{rr}}{dr} = 0 \tag{2.1}$$

Lamé [1852] provides a solution which satisfies this and compatability.

$$\sigma_{rr} = A - \frac{B}{r^2} \qquad \sigma_{\theta\theta} = A + \frac{B}{r^2} \tag{2.2}$$

Using this alongside the boundary conditions ($\sigma_{rr}(r = \frac{\phi}{2}) = -p$) and $\sigma_{rr}(r = c + \frac{\phi}{2}) = 0$, where c is concrete cover and ϕ bar diameter, and noting that $p = \tau \tan\alpha$ leads to Tepfers' solutions.

$$\sigma_{rr} = \frac{(\frac{\phi}{2})^2 \cdot \tau \cdot \tan(\alpha)}{(c+\frac{\phi}{2})^2 - (\frac{\phi}{2})^2}(1 - \frac{(c+\frac{\phi}{2})^2}{r^2}) \qquad \sigma_{\theta\theta} = \frac{(\frac{\phi}{2})^2 \cdot \tau \cdot \tan(\alpha)}{(c+\frac{\phi}{2})^2 - (\frac{\phi}{2})^2}(1 + \frac{(c+\frac{\phi}{2})^2}{r^2}) \tag{2.3}$$

As $r < c + \frac{\phi}{2}$, the radial stress will always be compressive, and the tangential tensile. The end of elastic behaviour will occur when a tensile failure occurs at the edge of the reinforcement, causing cracking. As such, it can be written that the maximum tensile stress (at $r = \frac{\phi}{2}$), is

$$(\sigma_{\theta\theta})_{max} = \frac{\tau \cdot \tan\alpha \left[(c+\frac{\phi}{2})^2 + (\frac{\phi}{2})^2\right]}{(c+\frac{\phi}{2})^2 - (\frac{\phi}{2})^2} \tag{2.4}$$

which can be rearranged, taking $\tan\alpha = 1$, to give a value of the bond stress at which cracking first occurs (where $(\sigma_{\theta\theta})_{max}$ equals f_{ct}.)

$$\tau_{elastic} = f_{ct}\frac{(c+\frac{\phi}{2})^2 - (\frac{\phi}{2})^2}{(c+\frac{\phi}{2})^2 + (\frac{\phi}{2})^2} \tag{2.5}$$

This gives an estimate of the elastic limit, below which the bar will return elastically to its original position upon unloading. The bond-slip relationship will be linear in this region.

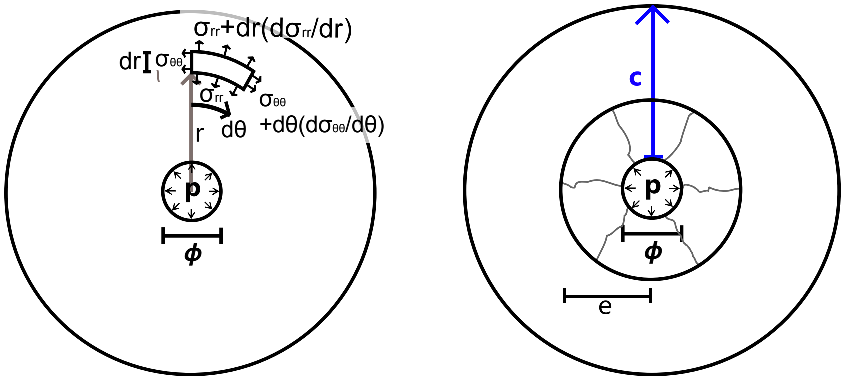

(a) Elastic Initial Stage (b) Partially cracked elastic

Figure 2.2: Tepfers [1973]

2.1.2 The partially cracked elastic stage

As cracks form, a cracked cylinder forms that bears no bond force, but instead transfers the radial force from the reinforcement bar to the edge of this cracked cylinder (Figure 2.2b), such that

$$\tau \cdot \tan(\alpha) \cdot \pi \cdot \phi = p_2 \cdot \pi \cdot 2e \text{ giving } p_2 = \frac{\phi}{2e} \cdot \tau \cdot \tan(\alpha) \tag{2.6}$$

where e represents the radius of cracking. Using Lamé's equation (Equation 2.2), the maximum tangential tensile stress at the edge of the cracked cylinder is

$$(\sigma_{\theta\theta})_{max} = \frac{\phi}{2e} \cdot \tau \cdot \tan(\alpha) \cdot \frac{(c+\frac{\phi}{2})^2 + e^2}{(c+\frac{\phi}{2})^2 - e^2} \tag{2.7}$$

Rearranging, setting $\sigma_{\theta\theta} = f_{ct}$ and $\tan(\alpha) = 1$ (as in Equation 2.5), an estimate for bond stress can be obtained

$$\tau = f_{ct} \cdot \frac{2e}{\phi} \cdot \frac{(c+\frac{\phi}{2})^2 - e^2}{(c+\frac{\phi}{2})^2 + e^2} \tag{2.8}$$

Setting $\frac{d\tau}{de} = 0$ shows that a maximum value of bond stress can be found of

$$\tau_{max} = f_{ct} \cdot \frac{(c+\frac{\phi}{2})}{1.664\phi} \quad \text{when } e = 0.486(c+\frac{\phi}{2}) \tag{2.9}$$

This provides an elastic lower bound on splitting failure.

2.1.3 Failure by splitting

Tepfers' work focuses on failure by splitting. This occurs as a result of tangential stresses away from the bar, which can be resisted by plastic behaviour in the cylinder. This approach provides an upper bound on failure. The most fundamental of these is for the cylinder shown in Figure 2.3a,

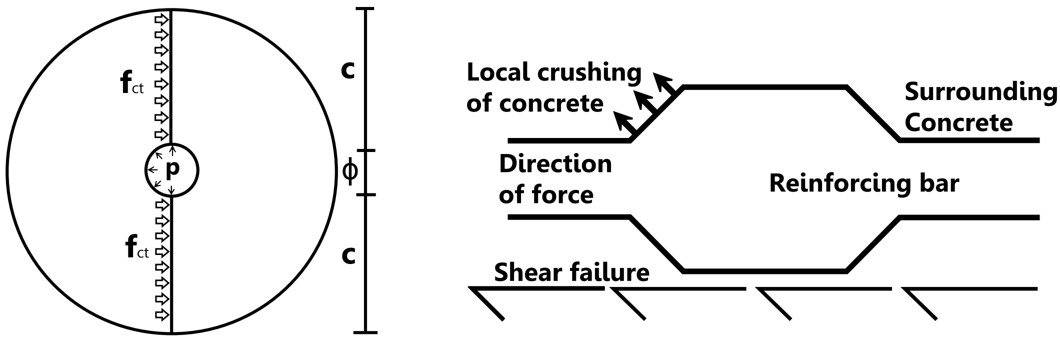

(a) Plastic upper bound on failure

(b) Pull out failure

Figure 2.3: Failure Mechanisms

$$2c \cdot f_{ct} = \phi \cdot \tau \cdot \tan(\alpha) \tag{2.10}$$

This can be rearranged to give the maximum bond stress

$$\tau_{plastic} = \frac{2c \cdot f_{ct}}{\phi} \tag{2.11}$$

Tepfers states that his equations can be applied to beams with c taken as representing the minimum concrete cover.

2.1.4 Pull-out failure

For bars with a reasonable cover-diameter ratio ($\frac{c}{\phi}$), pull-out failure will occur. This is where local crushing of concrete around the bar occurs due to the bond force, causing a shear plane to form. However, the small scale non-heterogeneous nature of concrete means it is difficult to formulate a theoretical equation for pull-out failure. As such, the equations that provide values are obtained through empirical work, reflecting the impact of cover and bond length. The most recent work on this subject was by the American Concrete Institute Technical Committee 408 [Darwin and Matamoros, 2003], which analysed a number of tests in order to improve previous formulae. They showed that the bond failure can be given by

$$\tau = \sqrt{f_{cu}} \left[0.1377 + 0.1539(\frac{c + \frac{\phi}{2}}{\phi}) + 2.673(\frac{\phi}{l_e}) + 1.053(\frac{h_r}{s_r}) \right] \quad \text{for } f_{cu} < 80MPa \tag{2.12}$$

2.2 The effect of confinement

Tepfers' bounds on failure assume the cylinder is unconfined. In half-joints and other reinforced concrete structures, this is not the case. Modifications to the existing models will be discussed and proposed later in this report in Section 8.

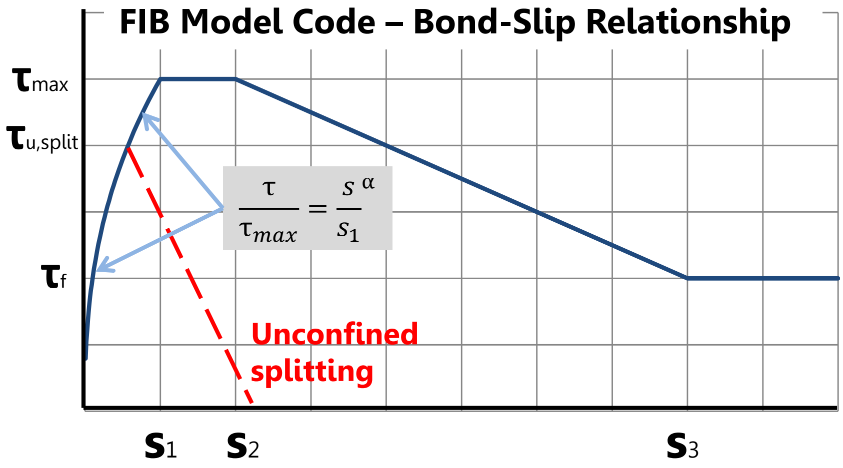

Figure 3.1: FIB 2010 Model Code Bond-slip relationship - FIB [2012]

	Pull-Out		**Unconfined Splitting**		**Confined Splitting**	
	Good Bond	*Other Bond*	*Good Bond*	*Other Bond*	*Good Bond*	*Other Bond*
τ_{max}	$2.5\sqrt{f_{ck}}$	$1.25\sqrt{f_{ck}}$	$7\left(\frac{f_{ck}}{20}\right)^{0.25}$	$5\left(\frac{f_{ck}}{20}\right)^{0.25}$	$8\left(\frac{f_{ck}}{20}\right)^{0.25}$	$5.5\left(\frac{f_{ck}}{20}\right)^{0.25}$
s_1	1.0mm	1.8mm	$s(\tau_{max})$	$s(\tau_{max})$	$s(\tau_{max})$	$s(\tau_{max})$
s_2	2.0mm	3.6mm	s_1	s_1	s_1	s_1
s_3	$c_{clear}{}^*$	$c_{clear}{}^*$	$1.2s_1$	$1.2s_1$	$0.5c_{clear}{}^*$	$0.5c_{clear}{}^*$
α	0.4	0.4	0.4	0.4	0.4	0.4
τ_f	$0.40\tau_{max}$	$0.40\tau_{max}$	0	0	$0.40\tau_{max}$	$0.40\tau_{max}$

* - c_{clear} is the clear distance between ribs

Table 3.1: Values for Bond-slip relationship curve - FIB Model Code 2010 - FIB [2012]

3 Previous Work

3.1 Force-slip behaviour of bond - FIB [2012]

Ultimate bond strength is only one characteristic of bond. It is also useful to evaluate the residual bond strength and the bond-slip relationship. The 2010 FIB Model Code FIB [2012], provides the most widely used model of bond behaviour, based on significant experimental work. This model separates failures into splitting and pull-out. It suggests pull-out samples will experience a parabolic increase in bond strength with slip up to a plateau at ultimate slip, before decreasing with further slip to a residual value equal to 40% of ultimate strength. Splitting failures will instead experience a sudden failure with a rapid drop to negligible bond stress. The generalised curve is shown as Figure 3.1 , and the factors are given in Table 3.1.

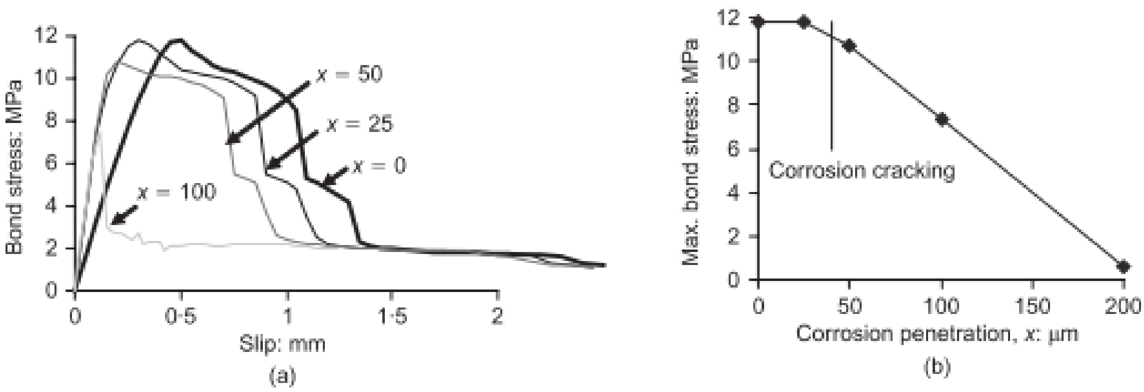

Figure 3.2: (a) Bond slip for different values of corrosion penetration. (b) Corrosion penetration depth against maximum bond stress. Taken from Lundgren [2007]

3.2 The effect of corrosion on bond

Lundgren [2007] presents a series of observations on the effect of corrosion on bond, based on Finite Element Models as well as proposed mechanisms of failure, shown as Figure 3.2. For ribbed bars with no transverse reinforcement, Lundgren suggests that a small amount of corrosion will have limited effect on the ultimate bond strength due to splitting failure. However, sufficient corrosion penetration into the reinforcement bar, resulting in cracking, will cause the bond strength to decrease. This analysis also shows that corroded reinforcement gives an initial stiffness of approximately twice that of uncorroded bars and this applies to all corroded specimens. This, alongside the lower values of ultimate slip shown, appears to contradict the FIB Code which suggests that poor bond conditions will experience greater slip. Finally, Lundgren shows that the residual bond stress is not altered by the presence of corrosion, although the ratio of $\frac{\tau_f}{\tau_{max}} \simeq \frac{2}{12} \simeq 0.17$ is greater than the zero value proposed for unconfined samples by FIB and therefore suggests that the actual residual bond for unconfined samples in splitting will be between 0 and the 0.4 specified for when stirrups are provided.

3.3 The effect of cracks on bond strength - Desnerck et al. [2015]

Considerable benefit would be gained from the ability to relate formation of cracks directly to bond strength. Desnerck et al. [2015] (in the Department of Engineering) performed a series of pull-out tests (see Section 4.1) on concrete cylinders. They show that a crack will cause the ultimate bond stress to fall to approximately 50% of its initial value (Figure 3.3a). They also suggested that the bond-slip stiffness is reduced by the presence of cracks, as shown in Figure 3.3b, whilst the ultimate slip reduces slightly with cracking. Residual bond is shown to be approximately 20% of ultimate bond.

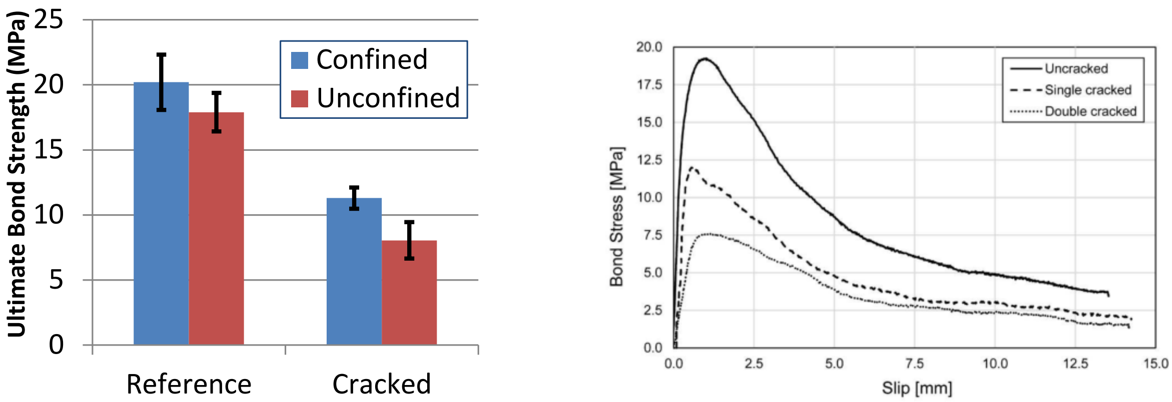

(a) Ultimate bond for cracked samples in pull-out

(b) Bond-slip relationship for uncracked, singly and doubly cracked samples - Figure taken from Desnerck et al. [2015]

Figure 3.3: Results from Desnerck et al. [2015]

Part II

Experimental method

4 Existing methods

Two main categories of method exist to allow experimental measurement of bond stress-slip behaviour: Pull-out and Beam tests. These are discussed below, with a view to deciding on a test method for this work.

4.1 Pull-out test

The Pull-out test was first proposed by Abrams [1913] and later codified by RILEM/CEB/FIB [1970]. It involves a cylindrical concrete sample with reinforcement protruding from the centre (Figure 4.1a). The sample is restrained by a plate at the top of the sample and the reinforcement pulled out. It allows quick and simple testing, often using an automated testing rig to allow accurate control of loadings and measurements. However, the method has disadvantages: Cairns and Plizzari [2003], amongst others, suggest that the concrete is placed in compression around the bond area, which is thought to give an increase in bond stress.

4.2 Beam test

At the other end of the complexity scale is the beam test. Again, it was proposed first by Abrams in 1913 and codified by RILEM/CEB/FIB in 1978. It consists of a four point bending test on a beam, with a hinge inserted to allow free rotation at the centre point, allowing

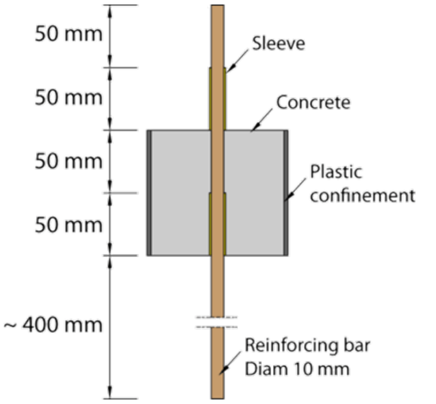

(a) Pull out test [Desnerck, 2011]

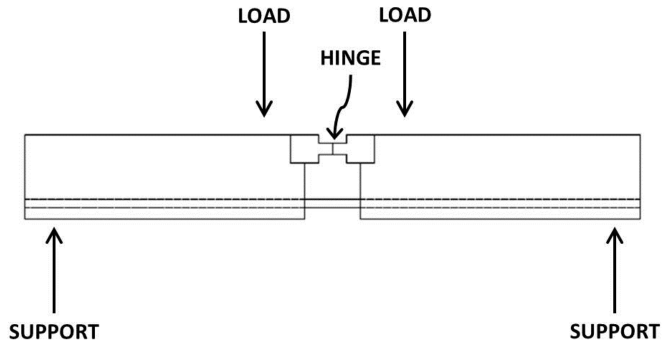

(b) Beam test

Figure 4.1: Methods of bond testing

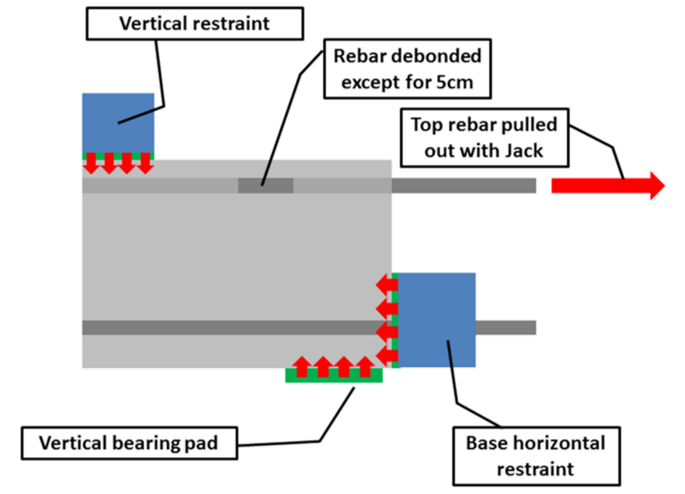

(a) Eccentric pullout (beam-end) test

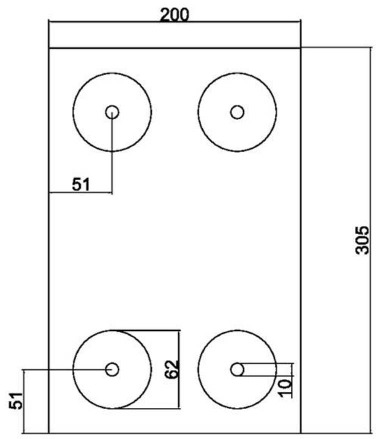

(b) Sample Dimensions

Figure 4.2: Test Setup

the reinforcement to slip in either half of the beam (Figure 4.1b). Whilst this method is a more accurate representation of beam behaviour, de Almeida Filho et al. [2007] showed that the two methods produced similar results, with ratios of $\frac{Bond\,strength\,(Pull\,out)}{Bond\,strength\,(Beam)}$ ranging from 0.798-1.257 for different samples. Soretz [1972] showed that there was no significant difference in the precision (scatter) of the results. Based on this, the beam test was not pursued for use in this work as the time taken to produce each sample, which requires full reinforcement for flexure and shear, would prevent enough tests being performed to allow meaningful comparisons in the limited timeframe.

4.3 The eccentric pullout (beam-end) test

Chana [1990] proposes a test method that offers a balance of accuracy and complexity. This consists (as shown in Figure 4.2a) of a rectangular block of concrete with reinforcement in all four corners (Figure 4.2b) that can be pulled out with a hydraulic jack. This is

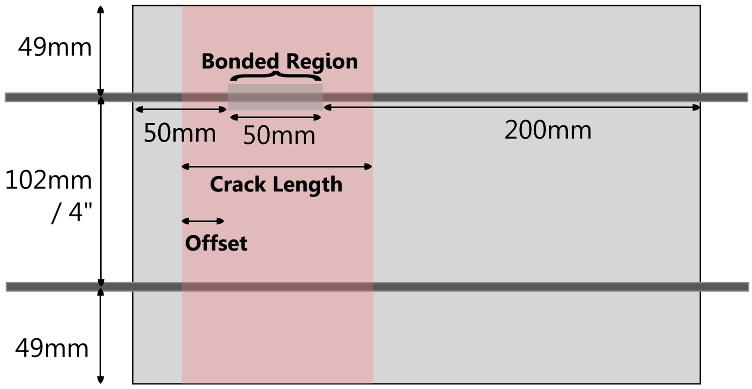

Figure 5.1: Plan view of sample, showing crack and bond length.
Crack Length is 100mm for Series 5 (centered equally), 300mm (whole surface) for Series 3. Bond length is always 50mm and location is the same for all tests.

shown by Chana to give results of bond strength similar to, or in excess of the characteristic values obtained from code equations.

5 Experimental setup

It was decided to perform tests using the Eccentric Pullout method as per Chana [1990]. It was planned to place cracks into the concrete, parallel to the reinforcement, through the use of precracked cylinders as well as plastic, oil and foil artificial crack methods. These were to be tested and the bond stress measured alongside the free end slip.

5.1 Sample dimensions and formwork design

A concrete sample of $305 \times 200 \times 300$mm was cast with four ø10mm reinforcing bars placed at 46mm cover in the corners of the sample. These dimensions are a result of the laboratory standard sections being in inches. Reinforcement was debonded by wrapping bars in layers of masking tape, except for a bonded length of 50mm on each bar (Figure 5.1). This layout is shown in Figure 4.2b. Formwork consisted of 18mm plywood and 3”x2” timber batons and was designed to interlock for additional strength.

5.2 Test setup & procedure

To perform the test, a setup using laboratory standard “meccano” sections was used (Figure 5.2). The block was restrained both horizontally and vertically (Figure 4.2a). A 50kN jack, restrained into the strong floor, was connected alongside a recently calibrated load cell and pressurised via a manual hydraulic pump. The free end slip between the reinforcement and concrete was measured using two LVDTs fixed to the reinforcement, which measured the distance to the concrete. These measurements were read into LabView by a

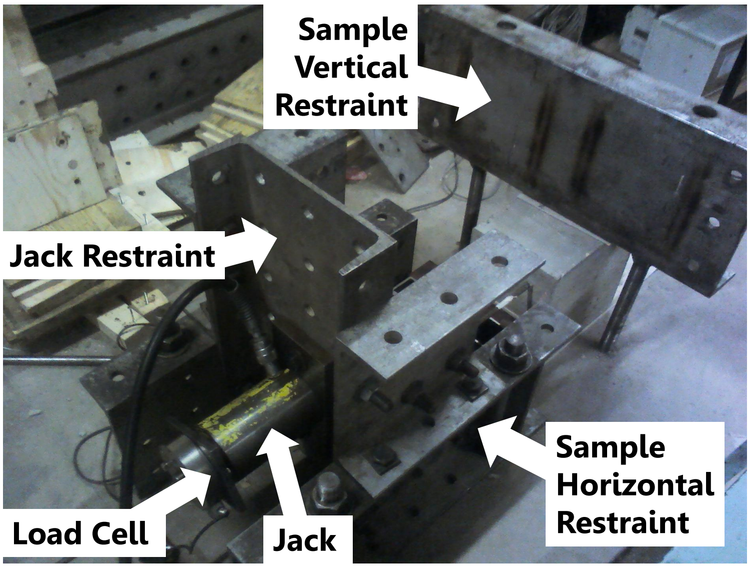

Figure 5.2: Test Rig

datalogger. Loading continued until approximately 10mm of slip had occured, so as to be in the middle of the working range of the 25mm LVDTs.

5.3 Cast information

5.3.1 Concrete details

A standard C30/37 concrete mix was used (as in Desnerck et al. [2015]), with a Water-Cement-ratio 0.60 and Sand-Coarse Aggregate ratio 0.45. Quantities used are given in Table 5.1. This concrete was found to have a slump of around 25-35mm. Concrete cubes and cylinders were produced to allow each cast to be tested, and the results from these are included at Appendix A and summarised in Table 5.2.

Ingredient	Amount (kg/m3)
Cement *CEM II/A-LL 32.5R*	300
Sand	835
Coarse Aggregate	1015
Water	180
Total Density	**2330**

Table 5.1: Concrete mix details

5.3.2 Cast List

The samples cast during the course of this work are detailed in Table 5.2. Diagrams showing the different casts are shown as Figure 5.3.

5.4 Sample Production

Two groups of casts were performed: Group 1 (December 2014) and Group 2 (February 2015). All casts (with the exception of the oil cracks, as detailed in Section 5.4.3) were cast in thirds, with concrete poured up to the level of the base reinforcement, vibrated,

Series	#	*Description*	*Cast date*	*Test date*	f_{cu}	f_{ct}
					(MPa)	
Group 1 (December 2014) Tests						
Series 1	x3	Uncracked control specimens - Table vibrated	17/11/14	9/12/14	31.8	3.17
Series 2	x3	62mm diameter pre-cracked cylinders	3/11/14*	10/12/14	29.6	3.10
Series 3a	x2	Artificial flaw - tin foil - full length of sample	27/11/14	11/12/14	23.8	2.66
Series 3b	x2	Artificial flaw - debonding oil - full length	27/11/14	11/12/14	27.1	2.43
Series 3c	x2	Artificial flaw - plastic - full length	27/11/14	12/12/14	24.0	2.39
Group 2 (February 2015) Tests						
Series 4	x3	Uncracked control specimens - poker vibrated	28/1/15	18/2/15	29.2	3.30
Series 5	x3	Artificial flaw - plastic - 100mm length	28/1/15	19/2/15	32.8	3.11
Series 6	x3	102mm diameter pre-cracked cylinders	28/1/15**	20/2/15	29.2	3.30

* - Cylinder Concrete cast 3/11, 'Fill' Concrete 17/11. ** - Cylinder 28/1 & Fill 10/2

Table 5.2: Cast List & summary of concrete strengths

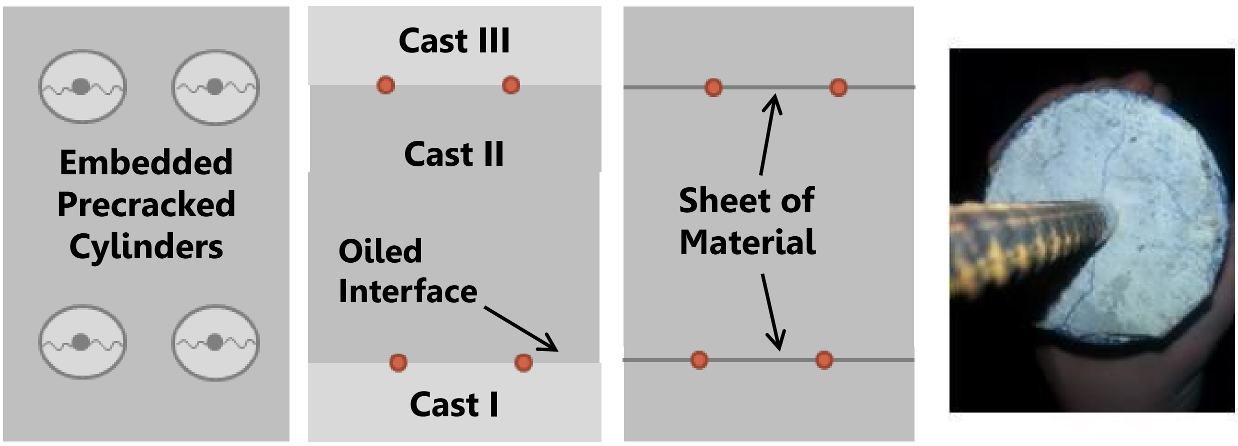

(a) (b) (c) (d)

Figure 5.3: Samples: (a) - *Embedded Cylinders* (2 & 6) | *(b) - Artificial Crack by debonding* oil (3b) | *(c) Artificial Crack by Silver Foil* (3a) and *Plastic* (3c & 5) | (d) - Photo of cracked cylinder

then filled to the top rebar, vibrated, and then filled fully before a final vibration and smoothing of the surface. Group 1 casts were vibrated on a vibrating Table until bubbles stopped appearing at the surface, usually after about 20 seconds. Group 2 casts used a vibrating poker for approximately 20 seconds for each third. Samples were left in formwork for approximately 24 hours, before being wrapped in clingfilm and stored at room temperature in the Structures Laboratory until testing. The two methods of placing cracks in the concrete are outlined below.

5.4.1 Cracks using pre-cracked cylinder

Series 2 and 6 utilised pre-cracked cylinders embedded into the concrete. These consisted of concrete cast into 100mm lengths of tubing with reinforcement passing through. Series 2 tests were formed from 62mm diameter drain piping, with an approximate wall thickness of 3mm. Series 6 tests were formed from thinner (1.5mm thickness) ventilation piping of 102mm diameter. Tape was applied such that only 50mm of the reinforcement was bonded.

These cylinders were then allowed to cure for one week before being pre-cracked by using a standard tensile splitting test setup on an automated testing rig (Figure 5.4b). The concrete was kept in its tubing to provide confinement to prevent the sample failing catastrophically. A displacement controlled test was performed, which was monitored and ended as soon as load was seen to drop off. This was taken to represent the time when cracks had formed. These cracks were identified on the sample with a pencil to ensure correct alignment in the block. An example of a cracked cylinder (from Series 2) is shown in Figure 5.3d.

These cracked cylinders were then embedded into the formwork (Figure 5.4a) and aligned such that the cracks were running horizontally with respect to the block (Figure 5.3a). This setup gives a “Crack Length” of 100mm and Offset of 0mm as defined in Figure 5.1. Concrete was then poured into the gap and vibrated as per Section 5.4.

5.4.2 Artificial Cracks - plastic and foil

Sample Series 3c and 5 used Sainsburys plastic cling-film as an artificial crack and Series 3a utilised Bacofoil aluminium foil, as shown in Figure 5.3c. These samples were filled to the level of the bottom bars and a precut sheet of the material placed on top of the concrete, covering the bars. In Series 3, these sheets were placed across the full area of the sample. In Series 5, the plastic was placed across the full width of the sample, but with a Crack Length 100mm centred around the area of bond (Offset = 25mm) (Figure 5.1). Concrete was then added to the level of the top rebar and vibrated. The process was then repeated before finally filling the block to the top of the sample.

(a) Embedded Cylinders

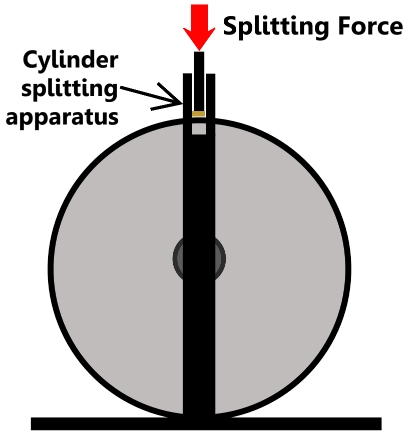

(b) Splitting test setup

Figure 5.4: Precracked cylinders

5.4.3 Oil Artificial Crack

Sample Series 3b consisted of an artificial crack formed by a multiple stage casting process. Concrete was first poured up to the level of the base reinforcement, vibrated and left for approximately 2 hours. Oil was then applied on the exposed surface and concrete poured up to the level of the top reinforcement. This was vibrated using a poker to ensure it did not disturb the partially set concrete underneath. After another 2 hour wait, the top surface was oiled and concrete poured up to the top of the mould, vibrated with a poker and smoothed.

Part III

Results and Discussion

6 Presentation of Results

A summary of results is presented in Tables 6.1 & 6.2. For each test, the applied pullout force, F_s and free-end slip were measured. Bond stress is calculated by assuming a uniform bond stress along the bonded circumference of the bar

$$\tau_{bond} = \frac{F_s}{\pi\phi \cdot l_e} \tag{6.1}$$

Three results are provided for each sample. The ultimate bond is the maximum bond stress reached during the test. The free end slip at this ultimate value is also measured. Characteristic bond strength is taken as the average of the bond stress at 0.01, 0.1 and 1mm of free end slip [RILEM/CEB/FIB, 1970]. Two ratios were calculated for each test series based on ultimate strength values in order to investigate top bar effect and the effect of failure of a bar on strength of adjacent bars.

A summary of the ultimate bond strengths are included as Figure 6.1. Further graphs of slip and characteristic Bond Strength are included in Appendix B. These graphs utilise a Retained Bond Factor for Ultimate & Characteristic strength. This is defined as the ratio of the ultimate bond of a particular sample to the ultimate bond strength of the corresponding "Uncracked" datum series (Series 1 for Group 1 tests, Series 4 for Group 2 tests). Refer to Table 5.2 for details of each series.

When stress-slip curves of different samples are compared hereafter, a single curve is used that is chosen to be representative of each series - these representative curves are shown as Figures 6.2 & 6.3. All curves obtained are shown as Figures B.3 and B.4, which shows which curve has been chosen for each series.

Sample Series	Bars	Ultimate Bond Strength		Characteristic Bond Strength		Slip at Ultimate Bond		Ultimate Strength Ratios	
		(MPa)	*Standard Deviation*	(MPa)	Std. Dev'n	(mm)	Std. Dev'n	$\frac{\textit{Top bars}}{\textit{Bottom bars}}$	$\frac{\textit{2nd bar}}{\textit{1st bar}}$
1 - Uncracked	*Top*	**4.6**	*0.44*	**3.2**	*0.70*	**1.22**	*0.34*	0.29	0.92
	Bottom	**15.9**	*1.58*	**9.9**	*2.07*	**0.69**	*0.14*		
2 - Cracked cylinders	*Top*	**15.5**	*1.3*	**8.2**	*0.80*	**0.96**	*0.22*	1.00	1.03
	Bottom	**15.5**	*2.73*	**8.1**	*1.74*	**1.05**	*0.21*		
3a - Foil Cracks	*Top*	**1.6**	*0.63*	**1.0**	*0.49*	**0.78**	*0.10*	0.50	0.68
	Bottom	**3.3**	*2.14*	**1.9**	*1.26*	**0.45**	*0.32*		
3b - Oil Cracks	*Top*	**3.2**	*1.27*	**1.8**	*0.89*	**0.90**	*0.36*	0.48	0.44
	Bottom	**6.6**	*4.75*	**4.1**	*2.65*	**0.37**	*0.26*		
3c - Plastic Cracks	*Top*	**2.0**	*0.19*	**1.2**	*0.12*	**1.05**	*0.27*	0.49	0.48
	Bottom	**4.0**	*1.44*	**2.1**	*1.06*	**0.38**	*0.29*		

Table 6.1: Group 1 Tests - Summary of Results

Sample Series	Bars	Ultimate Bond Strength		Characteristic Bond Strength		Slip at Ultimate Bond		Ultimate Strength Ratios	
		(MPa)	*Standard Deviaton*	(MPa)	Std. Dev'n	(mm)	Std. Dev'n	$\frac{\textit{Top bars}}{\textit{Bottom bars}}$	$\frac{\textit{2nd bar}}{\textit{1st bar}}$
4 - Uncracked	*Top*	**7.4**	*2.75*	**4.1**	*0.95*	**1.25**	*0.21*	0.43	0.90
	Bottom	**17**	*2.96*	**10.7**	*3.18*	**1.13**	*0.38*		
5 - Plastic Cracks	*Top*	**4.8**	*1.08*	**2.9**	*0.80*	**1.36**	*0.40*	1.04	1.16
	Bottom	**10.6**	*1.60*	**6.4**	*1.96*	**1.04**	*0.79*		
6 - Cracked Cylinders	*Top*	**10.8**	*2.55*	**5.6**	*1.41*	**1.22**	*0.22*	0.45	0.94
	Bottom	**10.4**	*1.78*	**5.6**	*1.25*	**1.28**	*0.32*		

Table 6.2: Group 2 Tests - Summary of Results

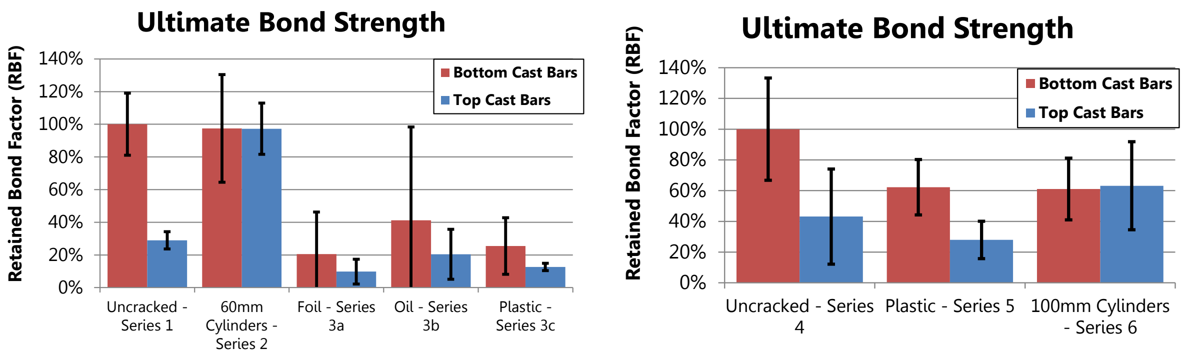

(a) Group 1 Tests

(b) Group 2 Tests

Figure 6.1: Ultimate bond strength. Error bars represent 95% confidence (1.94σ).

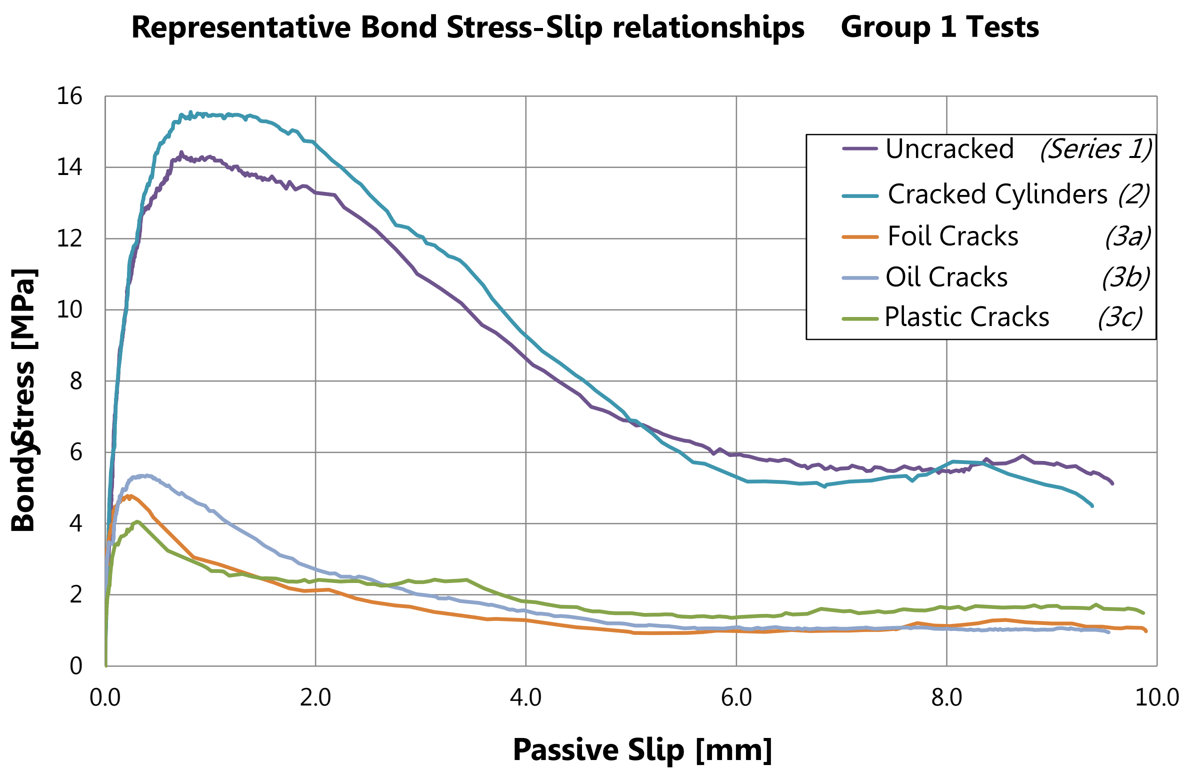

Figure 6.2: Representative Bond Stress-slip relationship - Group 1 - Dec. 2014

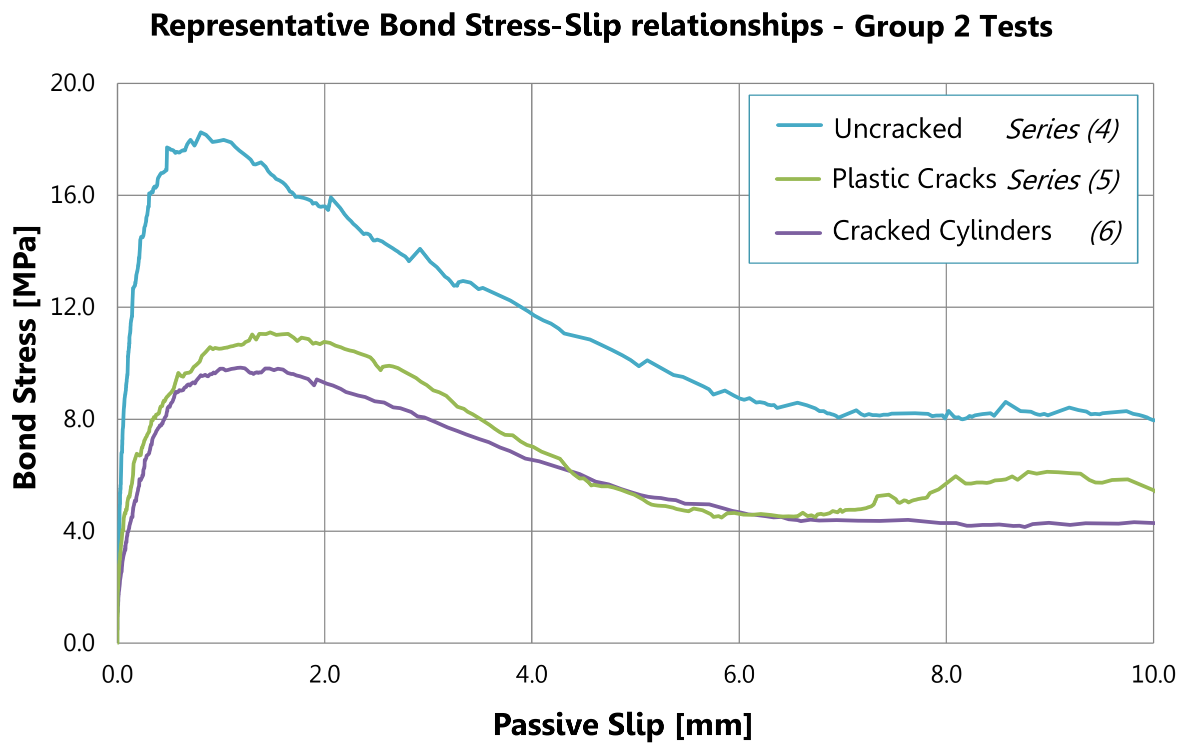

Figure 6.3: Representative Bond Stress-slip relationship - Group 2 - Feb. 2015

7 Results

The observed behaviour of our samples is outlined below. Certain areas of interest are then explored in greater detail.

7.1 Observed Behaviour

The results shown in Tables 6.1 & 6.2, and plotted as Figure 6.1 show an uncracked average ultimate bond strength of 15.9 and 17.0MPa for Series 1 and 4 bottom cast bars respectively. Embedded precracked cylinders with a crack radius of 30mm (Series 2) show a small decrease in ultimate bond strength of approximately 3%. For these samples, residual bond strength (taken to be the bond strength developed at 10mm slip) was observed to be approximately 40% of the ultimate bond strength (Figure 6.2) , and the pull-out failure observed had no effect on the strength of adjacent bars.

Artificial cracks along the whole surface of the sample (Series 3) provided a significant decrease in ultimate bond strength of approximately 60-80% and caused failure in splitting as opposed to the pull-out failure observed in uncracked and precracked cylinder samples. This splitting failure reduced the residual bond strength to approximately 25%, and caused a significant reduction in the strength of adjacent bars.

In the Group 2 tests, increasing the radius of cracking of cylinder samples to 50mm (Series 6) and providing the artificial plastic crack only along a 100mm length of the sample (Series 5) lead to comparable results, with a decrease of approximately 40% in ultimate bond strength compared to the reference uncracked samples (Series 4). These samples behaved similarly to the pull-out failures described above, however one sample failed in splitting.

In all cases, characteristic bond strengths showed similar relationships to those calculated from ultimate bond strength, and slip at ultimate bond was generally around 1mm, with some lower values due to splitting failure in Series 3 samples.

Tables 6.1 & 6.2 show that all sample Series, with the exception of cracked cylinder tests, experienced a significant “Top Bar Effect” where the top cast bars have a lower ultimate bond strength than bottom cast bars. The ratio of (Top Bar Strength)/(Bottom Bar Strength) is shown to be a maximum 50%, and a minimum of 28% (corresponding to a maximum and minimum reduction in capacity of 72% and 50% respectively). This effect is further shown in the Series 4 Stress-slip plots, shown as Figure 7.1. Uncracked datum blocks in the Group 1 tests (Series 1) were tested both top bars first and bottom bars first and no significant difference between results found, with top bars having 29% and 27% of the bottom bar strength respectively. For this reason, only bottom bars will be used for comparison purposes (except for cylinder Series 2 & 6).

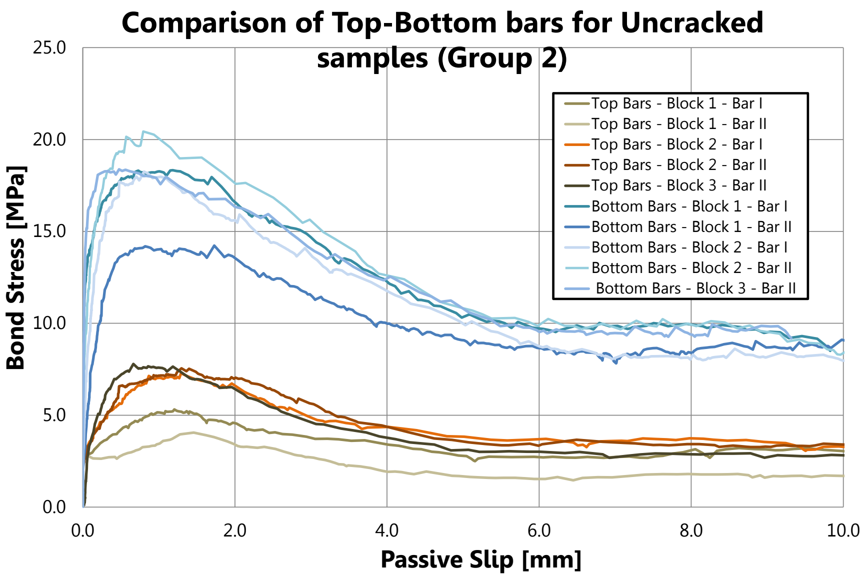

Figure 7.1: Bond stress-slip relationship - comparison between top & bottom bars - uncracked samples (Series 4)

Figure 7.2: Aluminium Crack sample at level of foil crack after testing

7.2 Artificial Cracks

7.2.1 Aluminium Foil Artificial & Oil Cracks

Approximately 2 hours after casting, small bubbles of gas were observed to have reached the surface of the Aluminium crack sample (Series 3a). These samples failed at low values in a splitting failure, with an accompanying significant drop in the strength of the bond of the second bar tested on a level. After testing, the concrete blocks split into three along the plane of the crack. It was observed that a chemical reaction had taken place, with the aluminium corroding in a reaction with hydroxides in the concrete (Figure 7.2). In view of this, foil was ruled out for any further use in this work, as the effect of this reaction on the localised concrete strength and bond behaviour is not known and is not likely to be encountered in the real world.

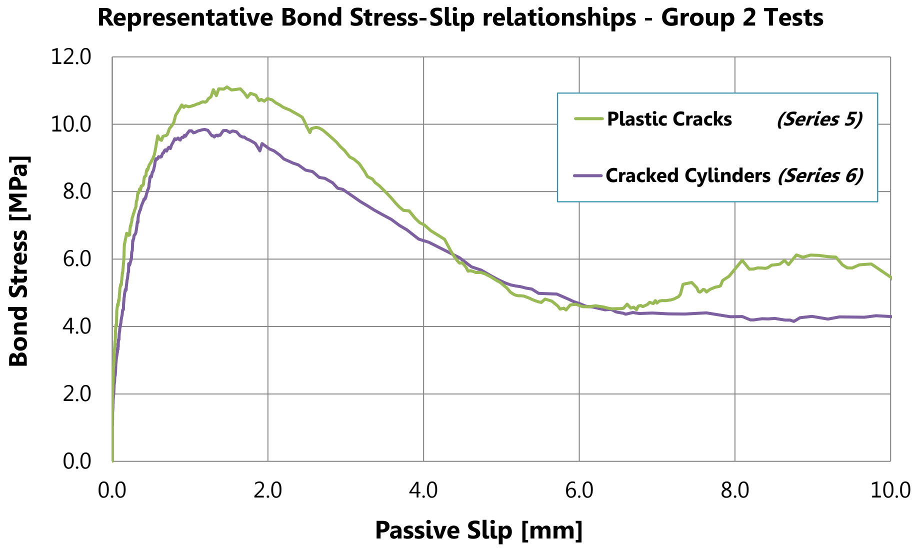

Figure 7.3: Representative Stress-slip relationship for cylinders & plastic cracks (Group 2)

In addition, oil cracks (Series 3b) were discounted as a method due to the high levels of error in these results, probably as a a result of the difficulty in adding a consistent quantity of oil and ensuring even set.

7.2.2 Validity of Plastic & Cylinder cracks

Group 1 tests showed a significant difference between Series 2 (cracked cylinders) and Series 3c (plastic cracks). Series 2 tests were found to have an ultimate bond strength 3.9x higher than Series 3c (plastic) and a characteristic strength 4.7x higher (Table 6.1). Slip at ultimate strength was also significantly lower for plastic cracks. This was a result of two factors (i) the initial cracked cylinders were $\phi 62$mm (crack radius 31mm), whereas the crack radius for the plastic was 50mm. (ii) The plastic was placed across the entire surface of the block, whereas the cylinder crack was only 100mm in length. This meant that Series 3 samples failed in splitting, whereas Series 2 samples failed in pull-out.

Group 2 tests overcame this by using $\phi 100$mm cylinders and 100mm crack length in the plastic. Figure 7.3 shows a strong similarity between the behaviour of $\phi 100$mm cracked cylinders (Series 6) and bottom cast plastic cracks (Series 5). Ultimate bond strengths are both 10.6MPa, characteristic strength 6.4MPa & 5.6MPa respectively and ultimate slip 1.04mm & 1.25mm (Table 6.2).

7.3 Adjacent Bars

Table 7.1 shows a ratio accounting for the effect of failure of one bar on the strength of adjacent bars on the same level. This reduction in 2nd bar strength is linked to the mechanism of failure. Results from Series 3 tests which failed in splitting suggest there

Series	1	2	3a	3b	3c	4	5	6	Average	
Failure Type (**P**ull **O**ut or **Sp**litting)	PO	PO	SP	SP	SP	PO	PO	PO	PO	SP
2nd bar / 1st bar ratio	0.92	1.03	0.68	0.44	0.48	0.90	1.16	0.94	0.99	0.53

Table 7.1: 2nd bar ratios (Bottom Cast Bars only)

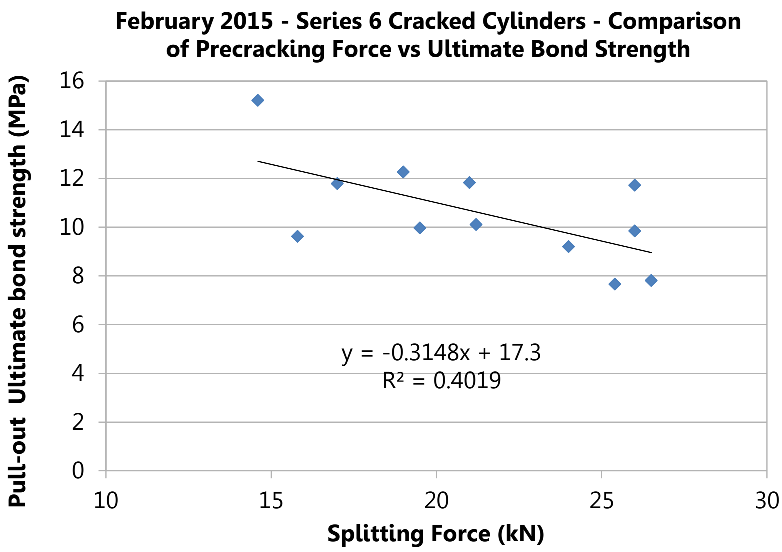

Figure 7.4: Graph of Precracking Force vs Ultimate bond strength - Series 6 (Group 2 Cracked Cylinder tests)

is between a 32% and 56% average loss of strength in the second bar. In these cases, the first bar causes a splitting failure to occur across the full length and width of the crack. This means any subsequent failure is unconfined, and the second bar experiences a pull-out style of failure between the bar and the concrete either above or below the bond (depending on which half of concrete the bar has remained attached to).

Pull-out failure is observed to have an insignificant effect on adjacent bar strength, as it is more of a localised failure. The variation on results is therefore attributed to the observed variation in bond stresses.

7.4 Cracked Cylinders - Precrack force

Figure 7.4 shows the relationship between the value of force required to split the cylinder in initial precracking and the resulting bond strength for Series 6 ϕ100mm cracked cylinders. The Coefficient of Determination of 0.4 suggests that 40% of the scatter in bond strength is accounted for by a linear relationship between these variables. It is thought that this is an indirect relationship, as a result of relationships between the width of crack and ulitmate bond strength as well as precracking force and crack width. Due to the placement of reinforcement in the cylinders, it was not possible to measure the crack width directly. This relationship is only significant for the 100mm diameter cylinders (Series 6).

In Series 2 samples (62mm cylinders), the coefficient of variation is <10%. There was also a higher variation in precracking results using the 100mm cylinders - a result of the thinner plastic cylinders used, which allowed more distortion as they provided less confinement. Were the cracked cylinder method pursued further, the use of thicker formwork plastic would appear to give more reliable precracking behaviour.

7.5 Test Method

7.5.1 Behaviour and Rigidity of Test Equipment

A concern over the method used was the risk of the concrete block rotating during testing and of the block lifting off from the ground, causing high concentrations of compressive stress at the front of the sample. Measurement of the horizontal deflection at the rear of the first sample block tested showed a negligible displacement of 0.001mm while a Dynamic Motion Measurement (DMM) setup confirmed that rotation and deflections of the support structure were negligible. No compressive crushing was observed.

7.5.2 Standard Deviation of Results

The results show high standard deviations. Standard deviation on Uncracked Sample ultimate bond strength was 1.58MPa for group 1 tests (Series 1) and 2.96MPa for group 2 tests (Series 4) (Tables 6.1 & 6.2). Two main reasons are identified: (i) Limitations in jacking equipment meant that the manual jacking force was difficult to control and often gave sudden increases in load. (ii) It is suspected the method of tape debonding used may have left surrounding reinforcement with partial bond, increasing the bond capacity and leading to misleading bond stress values. The high standard deviations of the results mean that these results are only suitable for drawing generalised conclusions, and specific values should be treated with caution for purposes of design and analysis.

7.6 Top Bar Effects

Tables 6.1 and 6.2 show a significant top bar effect was found, with top bars experiencing a reduction in ultimate bond strength of between 50-72% of bottom bar strength. In order to investigate this, the first uncracked sample (Series 1, block 1) was broken with a Concrete Hammer at the level of the bars and photographed (Figure 7.5). From this, it appears that there are more aggregates at the bottom than the top - this would be expected due to settlement of the aggregates. However, this alone does not explain the results.

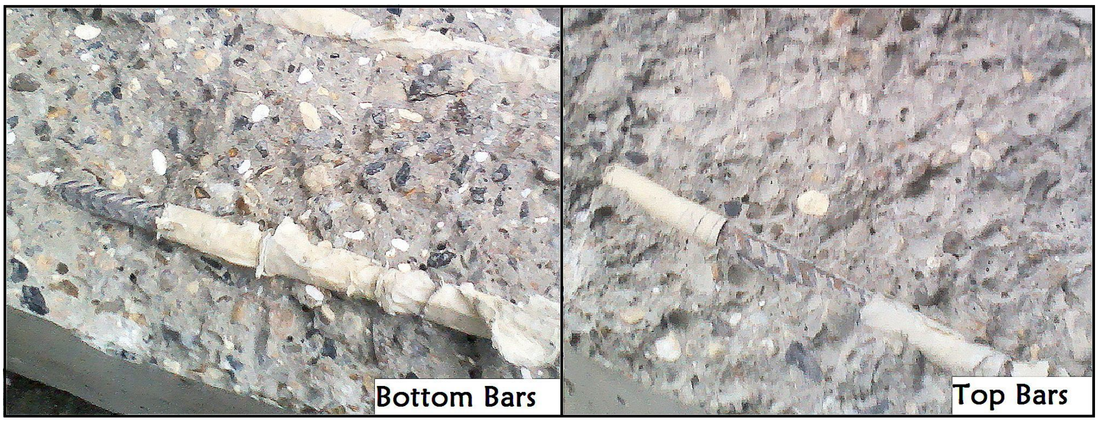

Figure 7.5: Photographic comparison of Bottom & Top bars concrete regions

7.6.1 Code provision for Top Bar Effect

Eurocode 2 [British Standards Institution, 2010] expresses bond strength as

$$f_{bd} = \eta_1 \eta_2 f_{ctd} \tag{7.1}$$

Where f_{bd} is the design ultimate bond stress (MPa), f_{ctd} is the design value of concrete tensile strength. η_2 is a coefficient related to bar diameter, and takes a value of unity for bar diameter less than $\phi 32mm$. η_1 is a coefficient relating to bond conditions and is 1 in "good bond conditions" and 0.7 in "all other cases". Any bar placed above 250mm from the bottom of the cast is considered poor. This suggests that a 30% reduction in bond strength can be expected in the top bars.

American Concrete Institution Code 318-11 [ACI Committee 318, 2011] makes a similar provision, although specifies an 30% increase in bond length, which corresponds to a 23% reduction in strength for top bars, similar to the 30% suggested by Eurocode 2.

7.6.2 Reasons for Top Bar effect

The top-bar effect observed in our tests is considerably greater than the 30% provided for in code provision. Possible reasons for this are discussed below.

7.6.2.1 Bleed of Water

Söylev and François [2006] performed a Series of pull-out tests on 10 bars embedded at different heights in a 2m high sample column. They produce the approximate relationships shown as Figure 7.6. Assuming the C20/40 behaves similar to the C30 used for our eccentric pull-out tests, it can be seen that in large samples, top bars will have negligible strength. However, using these results directly for our sample suggests the top bars should have a strength approximately 80% that of the bottom bars (Figure 7.6) , which is similar to the code provision. They suggest this is due to bleed of water from the concrete creating small voids, which are noticeable in our sample (Figure 7.5).

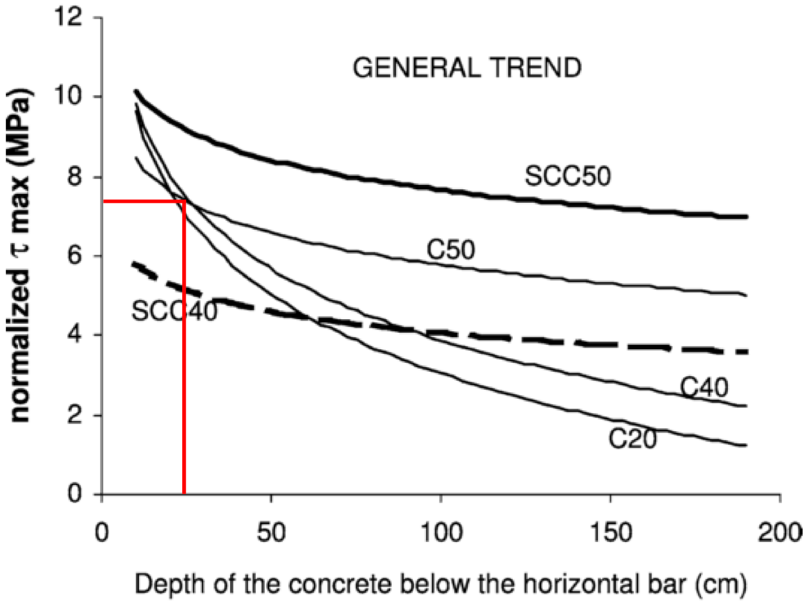

Figure 7.6: Relationship of Bond-Strength vs Cast location. Data for our test shown in red [Söylev and François, 2006]

7.6.2.2 Effect of Vibration

The casting of concrete can entrap air, which must be removed by vibration. It was thought the vibrating Table may not have provided sufficiently equal vibration, leading to a top bar effect in the Group 1 test samples. As such, Group 2 tests were vibrated with a poker instead as it was thought this would provide a more equal vibration over the height. This gave a small reduction in top-bar effect, but it was not significant. This agrees with work performed by Donahey and Darwin [1985] into the effect of vibration on the bond strengths of top-cast bars. They found that high-density vibration produced an increase in top bar bond strength over low-density vibration ranging from 0% to 23% for different conditions.

Repeating our eccentric pull-out tests with Self Compacting Concrete would confirm this is not a major factor.

7.6.2.3 Debonding

It was thought that the pressure of the overlying concrete may have caused the tape used for debonding to be compressed and behave as bonded, increasing the effective bond length and giving misleadingly high values of bond strength. This is discounted as were this true, we would expect to see a similar top bar effect in cracked cylinder samples, which was not observed.

7.6.2.4 Plastic Settlement Cracking

Welch and Patten [1965] performed a number of investigations into the effect of plastic settlement on bond behaviour. Plastic settlement can cause voids to form beneath reinforcement bars, and occurs as a result of shrinkage when the rate of evaporation of water

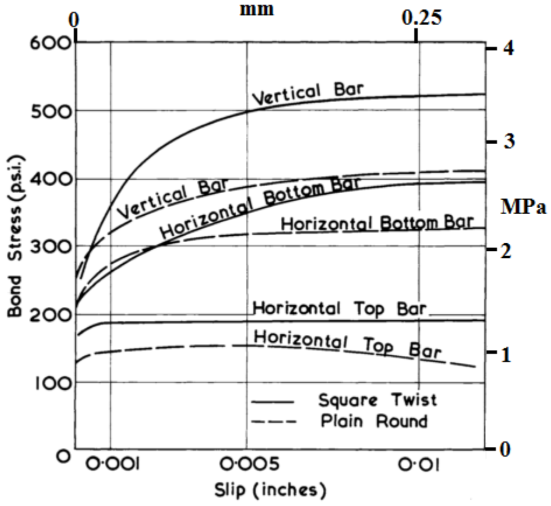

(a) Stress-Slip relationship for Top & Bottom Cast Bars

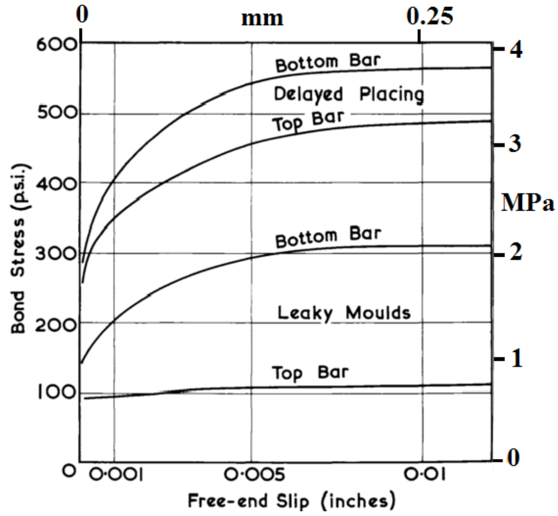

(b) Stress-Slip relationship for Round bars - Leaky moulds vs Delayed Placing

Figure 7.7: Graphs from [Welch and Patten, 1965]

from the surface is greater than the rate of bleeding in the concrete. Settlement can also occur as a result of leaky formwork causing cement paste to be lost at the bottom of the sample. Welch & Patten performed pull-out tests on a 300mm high block, with bars situated at 75mm from the top and bottom surfaces. These results were compared with bars cast vertically, which were assumed to represent the full (no-settlement) bond strength. Figure 7.7a shows a representative stress-slip plot for a standard block, whereby the reinforcement is not allowed to settle with the concrete. A significant top bar effect is noticed, with the top cast bars having ultimate bond strength approximately 30% (Round smooth bars) to 50% (square twisted bars) of the bottom cast bars, which is similar to our results.

In order to isolate this result as the behaviour of plastic settlement, a test was performed by Welch and Patten [1965] to compare the effect of using leaky wooden formwork (that could be expected to experience significant settlement due to leakage) with a smooth, well sealed metal formwork. This metal formwork was filled with concrete that had been allowed to rest for 40 minutes after mixing before casting to allow a significant portion of the bleed to occur prior to casting. Their results (Figure 7.7b) show a reduction in top bar strength of approximately 15% for no settlement and 67% for leaky moulds. As some leakage was noted during casting of our samples, it is thought these results may provide some explanation. Results from Desnerck et al. [2015] giving a pull-out ultimate strength of 19-21MPa can be seen as similar to the vertical stress from Welch & Patten (3.65MPa/530psi) in that these tests are unaffected by this settlement. This suggests that our results of ~17MPa (Tables 6.1 & 6.2) for uncracked (Series 1&4) samples are somewhere in between the 'smooth' mould and leaky mould, as we have seen a reduction in bottom bar strength relative to 'vertical' strength of approximately 15%, compared to a 40% reduction in bottom bar strength observed for leaky moulds by Welch & Patten.

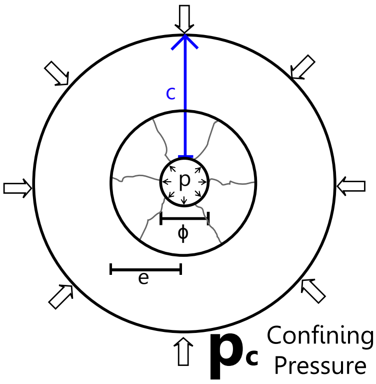

(a) Lower bound (Partially cracked elastic with Confinement)

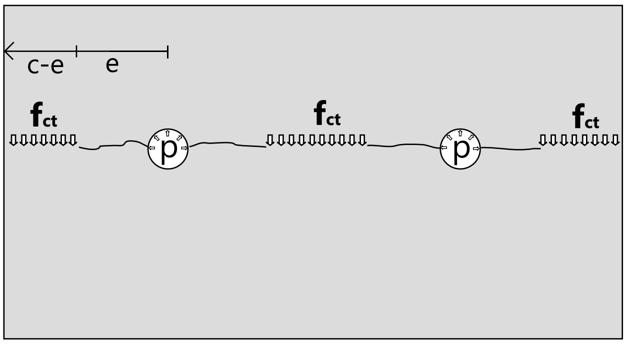

(b) Upper bound on failure (Cracked)

Figure 8.1: Splitting Failure Mechanisms

8 A Theoretical Approach for Cracked behaviour

Tepfers [1973] gives an explanation for the behaviour of the bond between uncracked concrete & steel (Section 2.1) This will be extended to cover cracked samples.

8.1 Initial behaviour

Tepfers' suggests uncracked samples will have an initial elastic stage with little slip prior to first cracking. This will not exist in cracked samples, as the crack is already present. Any load will therefore cause the crack to either grow in width or length.

It is possible to produce three values of the ultimate bond stress; a lower bound based on Tepfers' Partially cracked elastic splitting, an upper bound from Tepfers' plastic splitting model and a value corresponding to Pull-out failure.

8.2 Splitting Failure

8.2.1 Lower bound - Partially cracked elastic

$$\tau_{partially\ cracked} = (f_{ct}) \cdot \frac{2e}{\phi} \cdot \frac{(c+\frac{\phi}{2})^2 - e^2}{\cdot(c+\frac{\phi}{2})^2 + e^2} \tag{8.1}$$

Tepfers' Partially Cracked Elastic approach (Equations 2.8 & 8.1) can produce a value for bond strength in the presence of a a crack of radius e. However, it underestimates the bond stress at failure, sometimes significantly (Federation Internationale du beton (fib) [2000] & Section 9.2.2). Two improvements can be made to raise this lower bound towards the true failure values, thus accounting more accurately for cracked behaviour. An additional bond stress can be maintained as a result of cohesion in the cracked part of the cylinder - a number of studies have proposed solutions for this complex fracture mechanics problem. Some of these solutions are illustrated as Figure 8.2, and are seen to have the effect of stretching Tepfers' Cracked Elastic curve.

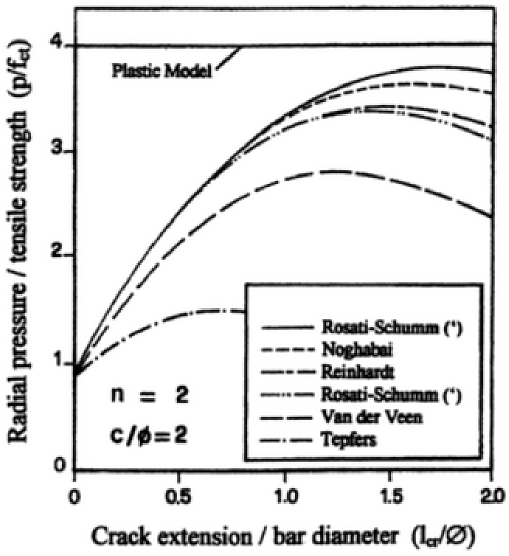

Figure 8.2: Plots of the bar-concrete pressure (radial pressure p) as a function of crack extension (l_{cr}). Φ = 19mm, c=38mm, f_c=32MPa. Different hyperbolic cohesive laws & different kinematic conditions in cracked core accounted for. *Taken from* [Federation Internationale du beton (fib), 2000]

Tepfers' equation is based on a 2-dimensional cylinder. In reality, there is concrete both surrounding the cylinder, and also in the regions away from the bonded area, which can behave in a manner similar to stirrups by providing confinement. This can be modelled as a confining pressure, p_c applied to the exterior of the assumed cylinder, as is shown in Figure 8.1a. Using the equations proposed by Lamé [1852] (shown in Equation 2.2), the following equation can be formed for partially cracked bond strength with external confinement.

$$\tau_{partially\ cracked} = (f_{ct}) \cdot \frac{2e}{\phi} \cdot \frac{(c+\frac{\phi}{2})^2 - e^2}{(c+\frac{\phi}{2})^2 + e^2} + \frac{2e}{\phi} \frac{p_c(c+\frac{\phi}{2})^2}{(c+\frac{\phi}{2})^2 + e^2} \tag{8.2}$$

The effect of this additional confinement term in Equation 8.2 is shown as Figure 8.3. It is therefore seen that the effect of increasing confinement has very similar effects to including cohesion, suggesting a possible empirical approach would be to group these two effects together.

8.2.2 Upper bound on splitting failure

Tepfers suggests a plastic collapse mechanism, shown as Figure 2.3a and evaluated as Equation 2.11. This can be adjusted to include cracked behaviour (Figure 8.1b).

$$\tau_{plastic} = \frac{2(c-e) \cdot f_{ct}}{\phi} + \frac{2ef_{t,cracked}}{\phi} + \text{Additional contribution from surrounding concrete} \tag{8.3}$$

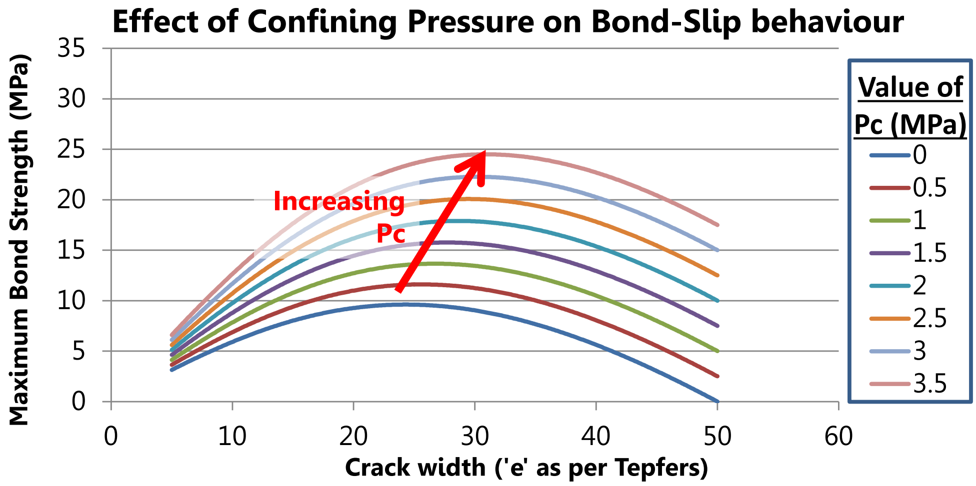

Figure 8.3: Effect of Increasing Confining Pressure on Ultimate Bond - Crack radius behaviour

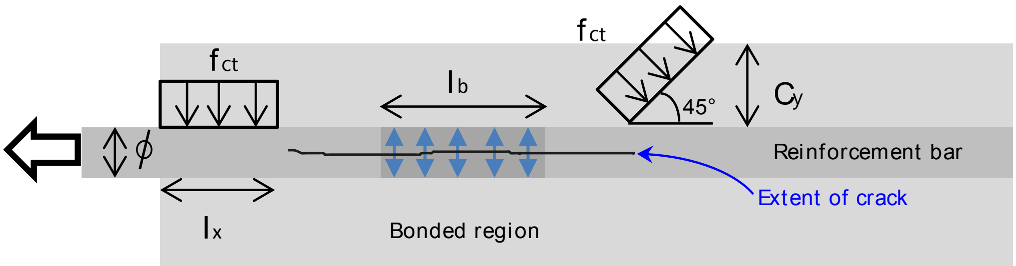

Figure 8.4: Upper bound on failure for crack (side view)

This equation suggests that the area immediately surrounding the reinforcement can develop full tensile capacity over the uncracked region and a very limited amount of resistance in the cracked region if the crack can sustain some tensile force. However, Tepfers' work focuses on a 2-dimensional section in the bonded region - equivalent to assuming an infinite bond length. In reality, the bond length is finite, and concrete surrounding the unbonded reinforcement can therefore give an additional increase in this strength.

Figure 8.4 provides a suggested means of calculating this upper bound on failure when a crack is present parallel to the rebar along part of the length, based on observed behaviour from our tests. In addition to the contribution from the concrete cylinder, the splitting bond stress will be restrained by tensile forces away from the bonded region. Splitting failure can either occur on the plane of the crack, as shown to the left of the diagram, or diagonally to the surface, as shown on the right - which failure occurs will be controlled by the shortest distance to a free edge. For example, on the left hand side of the diagram, failure will occur on the crack plane as $l_x < c_y$. On the right hand side, $c_y < l$ and therefore cracking occurs to the surface. These cracks are observed to be at approximately 45°. An equilibrium equation for this splitting failure can therefore be formed (Equation 8.4), which can be rearranged to give Equation 8.5 for the plastic upper bound on bond strength,

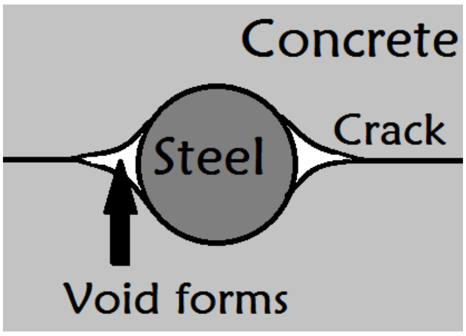

(a) Void formation around reinforcement

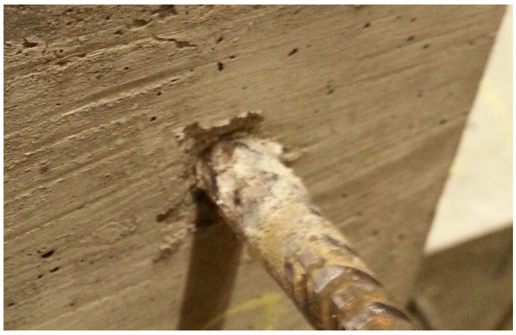

(b) Pull-out failure

Figure 8.5: Pull-out failure

$$\tau_{plastic} \cdot \phi \cdot l_b = 2c \cdot f_{ct} \cdot (l_x + \frac{c_y}{sin45} \cdot cos45) \tag{8.4}$$

$$\tau_{plastic} = \frac{2c \cdot f_{ct} \cdot (l_x + c_y)}{\phi \cdot l_b} \tag{8.5}$$

Where c is the minimum cover to the reinforcement (in any direction), and c_y is the vertical cover.

8.3 Pull-out Failure

Tepfers' lower bound covers splitting. The majority of our samples (with the exception of Series 3) failed in a Pull-out failure mode, characterised by a localised failure of the concrete surrounding the bar. As per Section 2.1.4, it is most common to use an empirical equation for pull-out failure. A possible explanation for the reduction in ultimate bond strength observed would be that cracks can open up and leave a small void - a region whereby there is no, or significantly reduced bond present around the bar, shown in Figure 8.5a. This would suggest that as these cracks grow, the full bond stress can only develop over part of the reinforcement, leading to a lower average bond stress.

This suggests that pull-out failure can be described by an equation of the form shown in Equation 8.6. In this case, the function X represents the percentage of full bond obtained. It will give a reduction in strength due to these voids forming as a result of cracks, which are thought to be related to the crack width and in turn the crack radius and bar diameter (Section 7.4). It will also be affected by confinement - Desnerck et al. [2015] suggests an 11% reduction in pull-out bond strength when confinement is removed.

$$\tau_{pull-out,cracked} = \tau_{pull-out,uncracked} \cdot X(e, \phi, c, p_c) \tag{8.6}$$

Further work using cracks of different sizes and different confinements could be performed in order to develop an empirical equation for this function.

Case	**Series 1 Experiments**	**Series 4 Experiments**	**FIB 2010 Model Code**	**ACI 408**	Desnerck [2015]
	Table 6.1	Table 6.2	Table 3.1	Equation **2.12**	
Ultimate Bond Strength (MPa)	15.9	17.0	13.7	8.7	19.9

Table 9.1: Pull-Out Failure of uncracked samples - comparison to theory & previous work

9 Comparison of Results & Theory

It is desired to compare our results to both existing theory and the modified cracked theory proposed previously. When performing calculations, a concrete compressive strength of 30MPa and tensile strength of 3MPa have been taken as representative. Cover is 45mm, and bar diameter 10mm in our tests, with a bond length of 50mm. Rib height was approximately 0.75mm, and rib spacing 7.5mm.

9.1 Pull-Out Failure

The behaviour of the uncracked reference samples can be modelled by Pull-Out failure equations, and are summarised in Table 9.1 The reference uncracked samples had an ultimate bond strength of 15.9MPa (Series 1) and 17.0MPa (Series 4) for bottom cast bars (Tables 6.1 & 6.2). Top cast bars produced significantly different results (Section 7.6). All specimens failed in pull-out, as expected. The FIB Model Code (Section 3.1, FIB [2012]) would suggest a value for pull-out failure of $\tau_{max} = 2.5\sqrt{30} = 13.7MPa$. The equation from ACI Technical Committee 408 (Darwin and Matamoros [2003], Equation 2.12) gives a value of $\tau_{pull-out} = 8.7MPa$.

$$\tau = \sqrt{30MPa}\left[0.1377 + 0.1539(\frac{45mm + 5mm}{10mm}) + 2.673(\frac{10mm}{50mm}) + 1.053(\frac{0.75mm}{7.5mm})\right] = 8.7MPa \tag{9.1}$$

Results from the eccentric pullout tests performed are therefore higher than both of these, however are lower than the average value of 19.9MPa for confined pull-out tests with $\phi 10$mm bars and cover of 45mm performed by Desnerck et al. [2015]. Slip at ultimate strength is generally around the 1mm suggested by the FIB Model Code, and the average characteristic strength of 10.3MPa is consistent with the values obtained by Desnerck (Section 3.3).

9.2 Splitting Failure

There are two approaches to calculating splitting failure; either using empirical equations, or Tepfers theoretical approach. These are shown in Table 9.2.

Case	**Series 3 Experiments**	**Series 5 Experiments**	**FIB 2010 Model Code**	**Tepfers** [1973]	**Tepfers** [1973]	**Tepfers** [1973]
	(Crack Length 300mm)	(Crack Length 300mm)	"Unconfined Good Bond"	Lower Bound No Crack	Lower Bound 30mm Crack	Upper Bound
	Table 6.1	Table 6.2	Table 3.1	Equation 9.3	Equation 9.4	Equation 9.5
Ultimate Bond Strength (MPa)	3.3, 6.6 & 4	12.5	7.7	9.0	8.8	27

Table 9.2: Splitting Failure - comparison to theory & previous work

9.2.1 FIB Model Codes

The FIB 2010 Model Code [FIB, 2012] provides an equation for calculating splitting failure (Table 3.1) for Good Bond Conditions, which are assumed to be unconfined

$$\tau_{split,good,confined} = 7 \cdot \left(\frac{30MPa}{20MPa}\right)^{0.25} = 7.7MPa \tag{9.2}$$

This value is between the observed Ultimate Bond Strengths for Series 3 (3.3, 6.6 & 4MPa for Series 3a, 3b, 3c respectively, from Table 6.1) and the value of 12.5MPa, at which a single Series 5 sample experienced splitting failure.

9.2.2 Lower bound - Tepfers Partially cracked elastic

Tepfers' lower bound approach (Equation 2.9) for splitting suggests the radius of cracking will increase up to a critical value as bond stress increases. Applying this equation to our samples gives

$$\tau_{max} = f_{ct} \cdot \frac{c + \frac{\phi}{2}}{1.664\phi} = 3 \cdot \frac{50}{1.664(10)} = 9.0MPa \tag{9.3}$$

For cracks smaller than the critical crack of $0.486 \cdot 50mm = 24.3mm$ (Equation 2.9b), they will develop this maximum bond stress. For cracks larger than this, the crack radius can be used in Equation 2.8 to give a lower bound on failure. For 30mm cracks:

$$\tau = f_{ct} \cdot \frac{2e}{\phi} \cdot \frac{(c+\frac{\phi}{2})^2 - e^2}{(c+\frac{\phi}{2})^2 + e^2} = 3MPa \cdot \frac{2(31)}{10} \cdot \frac{(50)^2 - 30^2}{(50)^2 + 30^2} = 8.76MPa \tag{9.4}$$

By inspection, 50mm cracks will give a zero bond strength. This is therefore correct as a lower bound, however there are two major inconsistencies: (i) Both values of bond strength for 30mm cracks & uncracked are significantly below our values. (ii) It predicts a zero bond strength for 50mm cracks, versus an observed bond strength of 10.6MPa (Table 6.2.)

(a) Image of splitting failure across whole length crack

(b) 100mm crack length plastic specimen

Figure 9.1: Splitting failure

9.2.3 Upper bound - Plastic

Tepfers suggests a plastic collapse mechanism, shown as Figure 2.3a. For our sample, this gives the upper bound

$$\tau_{plastic} = f_{ct}\frac{2c}{\phi} = \frac{2(45mm)\cdot 3MPa}{10mm} = 27MPa \tag{9.5}$$

This value is seen to be considerably higher than any of the results obtained in our tests, as would be expected.

9.2.4 Cracked Theory - Lower bound for splitting

In Section 8.2 a theoretical approach to cracked behaviour was proposed. This can be applied to our cracked samples in order to raise the lower bounds given in Section 9.2.2. Two types of splitting failure were observed in our tests. Series 3 samples with full length cracks of radius 50mm failed as shown in Figure 9.1a. In this case, there is no confinement, and thus the bond is a result of cohesion in the cracked region. One Series 5 Plastic (50mm crack radius, 100mm crack length) sample failed in splitting, as shown in Figure 9.1b - in this case, the surrounding concrete is likely to provide confinement. Series 2 cracked cylinders (radius 30mm) failed in pull-out, and therefore cannot be evaluated using this approach. Equation 8.2 can be used to find a value of confining pressure that matches the results obtained in our experiments

$$\tau_{series-3} = (3MPa)\cdot\frac{2(50)}{10}\cdot\frac{(45+5)^2-50^2}{(45+5)^2+50^2} + \frac{2(50)}{10}\frac{0.92MPa(45+5)^2}{(45+5)^2+50^2} = 4.6MPa \tag{9.6}$$

$$\tau_{series-5} = (3MPa)\cdot\frac{2(50)}{10}\cdot\frac{(45+5)^2-50^2}{(45+5)^2+50^2} + \frac{2(50)}{10}\frac{2.5MPa(45+5)^2}{(45+5)^2+50^2} = 12.5MPa \tag{9.7}$$

A confining pressure equal to 2.5MPa is seen to represent the Series 5 result, failing in splitting at a bond stress of 12.5MPa, whilst a confining pressure around 0.92MPa would match our Series 3 sample results, which failed at an average 4.6MPa (Table 6.1) - this can be thought as representing the contribution from cohesion, as the cylinder is largely unconfined.

9.2.5 Cracked Theory - Upper bound for splitting

It is possible to use Equation 8.5 to calculate an upper bound on the Series 5 splitting failure for a 100mm length crack, which matches the observed failure mechanism (Figure 9.1b)

$$\tau_{plastic} = \frac{2 \cdot 45mm \cdot 3MPa \cdot (25mm + 45mm)}{10mm \cdot 50mm} = 37.8MPa \tag{9.8}$$

This value, as expected is significantly above the observed failure at 12.5MPa, suggesting that this surrounding concrete does not develop full strength. A similar equation cannot be formed for the Series 3 failures with cracks along the whole length of the sample, as it would involve assuming a tensile force across the cracks.

9.3 Comparison with Design Codes

Eurocode 2 [British Standards Institution, 2010] expresses bond strength as Equation 9.10. Table 5.2 suggests our concrete had a mean tensile strength of 3MPa and an approximate standard deviation of 0.2MPa. Eurocode 2 therefore requires use of a design tensile strength of

$$f_{ctd} = \frac{f_{ct,k,0.05}}{1.5} = \frac{3 - 1.94(0.2)}{1.5} = 1.74MPa \tag{9.9}$$

Where $f_{ct,k,0.05}$ is the characteristic tensile capacity of the concrete, above which 95% of results fall. Considering good bond conditions ($\eta_1, \eta_2 = 1$), this gives a value for design bond strength of

$$f_{bd} = \eta_1 \eta_2 f_{ctd} = 1 \cdot 1 \cdot 1.74MPa = 1.74MPa \tag{9.10}$$

This value of 1.74MPa is considerably lower than the majority of results obtained. It is thought that this is a result of two approaches of code design: Firstly, it is desirable to ensure slip is limited to a negligible value (~0.01mm), hence the design stress ought to be in, or close to the elastic limit. Alternatively, in order to introduce further safety, it is thought design should use the residual bond strength. Both of these approaches introduce a significant factor of safety, which means that effects such as micro-cracking, voids underneath bars and some corrosion are allowed for in the design capacity. Our results therefore agree with the conclusion of Desnerck et al. [2015] that the code has, albeit not explicitly allowed for there to be some cracks along the length of the bar. This

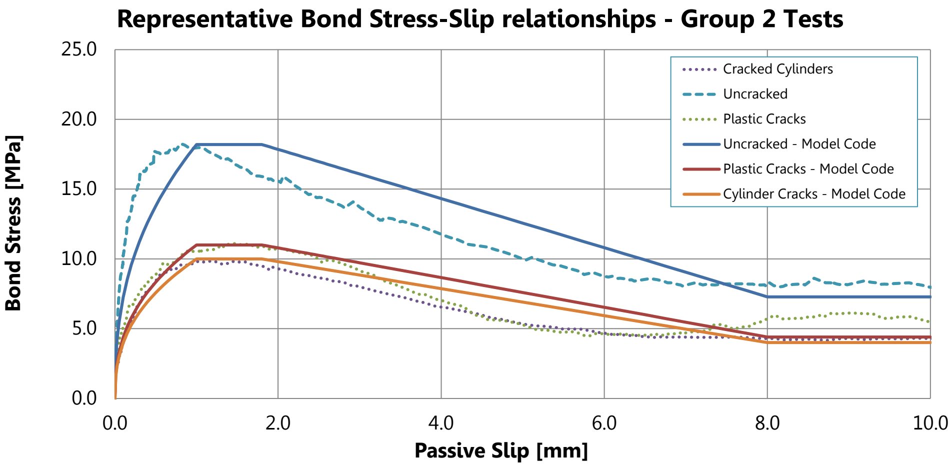

Figure 9.2: Group 2 representative stress-slip relationships compared to FIB 2010 Model code equations (α=0.4)

suggests that some cracking can occur and full code bond strength be developed, although this would result in the first condition of low slip being partially broken.

9.4 Bond stress-slip Behaviour of Cracked Samples

It is desirable to have an understanding not just of values for ultimate and characteristic bond, but also the relationship between bond stress and slip. The slip at ultimate bond can give an idea of the ductility of the failure, however it is useful to have a full relationship, which allows the slip to be calculated for a given bond stress. In this section, and in Figure 9.2, the value of τ_{max} for plotting the code equation is the ultimate bond strength of the particular sample that is chosen as representative. It is hoped this value could be calculated from a suitable equation, as proposed in Section 8. The purpose of this section is therefore to propose a model of slip based upon a calculated value of τ_{max}.

9.4.1 Bond slip behaviour - up until ultimate bond

All samples experience an initial linear region whereby a bond stress is mobilised with little or no slip. This region appears to extend up to a bond stress of approximately 2MPa. This linear-elastic region corresponds to the elastic solution proposed by Tepfers [1973]. Equation 2.5 gives a value of Bond Stress at first cracking of

$$\tau_{elastic} = f_{ct}\frac{(c+\frac{\phi}{2})^2-(\frac{\phi}{2})^2}{(c+\frac{\phi}{2})^2+(\frac{\phi}{2})^2} = 3MPa\frac{(50)^2-(5)^2}{(50)^2+(5)^2} = 2.94MPa \tag{9.11}$$

After this initial linear elastic region, the bond stress-slip behaviour is approximately parabolic, and appears to correspond well with a relationship of the form $\tau = \tau_{max}(\frac{s}{s_1})^{\alpha}$, as is proposed in the FIB 2010 Model Code FIB [2012]. This proposes a value of $\alpha = 0.4$ for all bond conditions. Figure 9.2, suggests that our results, both for cracked and uncracked

Series	1	2	3a	3b	3c	4	5	6	Average	
Failure Type (**P**ull **O**ut or **Sp**litting)	PO	PO	SP	SP	SP	PO	PO	PO	PO	SP
Residual Bond (%)	43	35	24	22	29	48	45	45	43	25
Standard Deviation (%)	5	4	9	16	2	6	6	10	8	10

Table 9.3: Residual Bond Strengths

behaviour broadly follow this behaviour, although a lower value of α may offer a better representation, however using 0.4 would provide a conservative (for estimating slip at a given bond stress) approach.

9.4.2 Bond behaviour - ultimate strength 'peak'.

The FIB Model code suggests that ultimate bond strength will occur over a region of slip from 1mm to 2mm for good bond conditions. Results from testing (Tables 6.1 and 6.2) are at the lower end of this range - values of slip at ultimate bond range from 1.04mm to 1.36mm for sample Series 1, 2, 4, 5 & 6, which all failed in pull-out failure. Samples which failed in splitting (3a, 3b & 3c) are observed to have a lower slip at ultimate bond, ranging from 0.37mm to 1.05mm. The FIB Model code suggests that this failure will occur at approximately 0.24mm for Good Bond conditions, and 1.04mm for "other" bond conditions.

9.4.3 Residual bond strength

The FIB Model code suggests a residual bond strength (after failure) for ribbed reinforcing bars equal to 40% of ultimate strength, mostly as a result of aggregates interlocking with ribs. Our data for both cracked & uncracked specimens tends to agree with this. Table 9.3 shows that Pull-Out failures had an average residual bond strength of 43% of the ultimate.

Splitting failures, as expected, have a much lower residual bond strength of around 25%. The model code specifies zero residual bond for splitting failures *without confinement*, however our data agrees with Lundgren [2007] (Figure 3.2) in that there is a small residual bond after splitting failure.

Finally, as can be seen in Figure 9.2 and in Appendix B, plastic and foil samples (3a, 3c & 5) experienced a small increase ($\sim$10%) in residual bond as slip increased towards and above 10mm. This is thought to be a result of the plastic/foil scrunching up infront of the ribs of the bar providing an additional frictional resistance and should be discarded as a quirk of this method of producing artificial cracks.

Part IV

How can Deteriorated Concrete Half-Joint Structures be Assessed?

10 Design implications of work & Further work required

As a result of the high standard deviations and the limited amount of tests performed, it would not be appropriate to propose definitive design equations. However, general observations can be made and future work suggested.

10.1 Calculation of pull-out and splitting failure values

In order to confirm the belief that the full design bond can often be developed in the presence of cracks along the reinforcement (Section 9.3), it would be useful to have a series of equations that are able to predict the failure mode and ultimate bond strength. This would give the engineer confidence that this assumption is correct. Splitting failure is largely related to the ratio of crack radius to cover, whereas pull-out failure is thought to be related mostly to crack radius and bar diameter. As a result of this, splitting failure will dominate failure of low cover/diameter ratio samples, whereas pull-out will dominate high cover/diameter ratios.

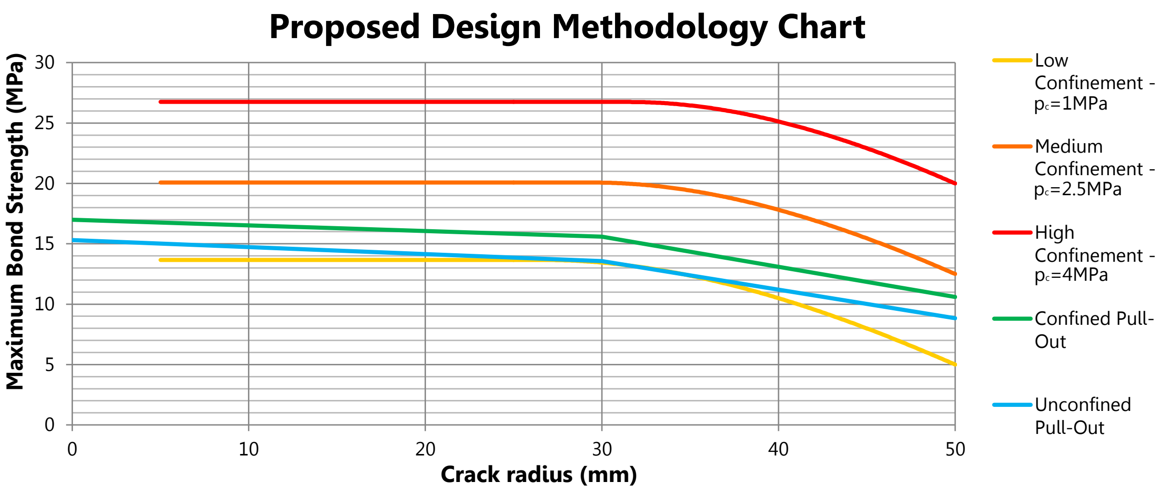

Figure 10.1: A possible approach to calculating bond strength with cracks

10.1.1 Splitting failure

Results from splitting failure are thought to be explained partly by Tepfers' partially cracked approach, as detailed in Section 2.1.2 and extended in Section 8.2. It would appear cohesion can be modelled as a confining pressure, as this may be more straightforward than Fracture Mechanics approaches. As confining pressure is difficult to quantify in practical situations, an approach whereby confinements are categorised (High/Medium/Low) corresponding to increasing confining pressures in Equation 8.2, could be used alongside empirical rules (based on further experiments) for which curve to use. These curves are shown in Figure 10.1. In the absence of cracks, or where a crack radius is smaller than the critical ratio, cracks can be thought to grow until they reach the critical crack radius, at which point they develop maximum splitting resistance.

An upper bound mechanism, as in Section 8.2.2 should be checked. This should be considerably higher than the actual failure value, however, is useful as it can suggest the likely failure mechanism.

10.1.2 Pull-out failure

An appropriate equation, such as that proposed by FIB [2012] or American Concrete Institute Technical Committee 408 [Darwin and Matamoros, 2003] can be used to calculate pull-out failure. This work suggests these underestimate the pull-out strength, although this is useful for design as it would ensure that variability between bond is accounted for. It is suggested that an equation of the form proposed in Equation 8.6, could be used to take account of confinement and any crack present. This requires further work to understand the effects of these two factors on bond strength and to develop empirical equation that fit a larger sample of data. Two approximate curves, based on our limited results for confined pull-out tests, and using the finding from Desnerck et al. [2015] that confinement gives an 11% increase ultimate bond strength are shown in Figure 10.1. It is thus thought that the effect of confinement is less for pull-out than splitting failure.

10.2 Factors of Safety

For an engineer to be confident in equations predicted, it would be necessary to include factors of safety. This would have two implications.

- Characteristic ultimate bond strength would need to be used - this is the value above which 95% of values would fall, and is based on using the mean and standard deviation values as $f_{b,ult,char} = f_{b,ult,mean} - 1.96\sigma$. The graphical approach provided in Figure 10.1 uses mean values of ultimate bond strength, and would therefore need more work to be adjusted to these characteristic values. It is felt that, whilst data from these tests could be used, the high standard deviations and comparatively limited amount of data obtained suggest errors in testing beyond those from variability in bond strength.

- In addition to this, convention dictates a partial factor on bond strength should be applied. In doing this, I would suggest it is necessary to consider the effect of adjacent bars. Pull-out failure does not have a significant affect on the bond strength of adjacent bars, whereas splitting failure causes a reduction of 32-56% reduction of bond in adjacent bars, and also only sustains 20% of bond strength after failure, compared to 40% for pull out failure. As such, it would be anticipated that a higher factor should be used against splitting failure.

The destructive nature of splitting, causing a lower residual bond and greater reduction in adjacent bar strength compared to pull-out failure is such that splitting will often control analysis, despite a pull-out failure being the observed failure mechanism.

11 Conclusions & Suggestions for Future Work

An area of concern in analysing half-joint bridges is the presence of cracks along the reinforcement bars in the anchorage regions. This project sought to devise and perform a series of tests to evaluate the effect of these cracks on the behaviour of bond.

The eccentric pull-out test is shown to give similar values to pull-out tests, yet allows testing of specimens more similar to real beam behaviour and has potential for testing multiple bars at once. The test setup was found to be sufficiently rigid, prevented rotation of the sample block and did not appear to cause crushing of concrete around the supports. The high standard deviation is thought to be down to errors in debonding and due to the jack setup. Further tests should use a more thorough method of debonding, such as tubing (which was not easily available for these tests) and would seek to use a hydraulic jack with more control at small load increments, potentially with computer-control.

Initial attempts to use aluminium and debonding oil to produce artificial cracks were discounted due to chemical reactions and high variability of results respectively. Using plastic “Cling-film” appeared to have some merit from initial tests, and further tests showed a strong correlation between results using these artificial plastic cracks and the cracked cylinder approach. It is thought that this method of utilising plastic could have significant advantages in future, due to the speed and ease of implementation and the ability to accurately control factors such as crack width, crack orientation and crack radius better than when using cracked cylinders. Tests also showed the importance of accurately modelling the length of crack either side of the bar, as this can have a significant effect on the splitting failure of the concrete due to the confinement provided.

It is thought that the observed top bar effect, causing between a 50% and 72% drop in top bar strength was a result of a series of circumstances present in this test that are not likely to occur during construction and it is thus inappropriate to comment on the validity of the code provision for a 30% reduction. However, these results reinforce that care should be taken to ensure good curing and sufficiently leak free formwork, both when performing tests in a laboratory and when on a site in order to avoid plastic settlement occurring. Where there is concern over plastic settlement, perhaps due to observed leakage shortly after casting, it is thought a revibration of concrete may be used to remove some of the voids formed by this plastic settlement beneath the bars. This would need further work to understand when and for how long this ought to take place.

It is shown that a crack can have a significant impact on bond strength. There appears to be a crack radius below which there is a negligible decrease in both ultimate and characteristic bond strengths - our experiments showed that a 30mm crack radius gave a negligible 3% decrease in ultimate bond strength. Above this critical value, a crack to the surface (radius of 50mm) of the test specimen is shown to reduce bond by approximately 40%. Failure can occur either by splitting or pull-out failure; splitting failure is shown to be modellalble by a version of Tepfers' [1973] Partially Cracked Elastic equation, modified to account for confining pressure as a result of surrounding concrete. This is thus dependent on both the crack radius and crack length. Pull-out failure is thought to be affected by a reduction in the amount of contact between the steel and concrete, as the crack opening causes a void to form, preventing full bond stress building up around the full circumference of the bar. Further work could be performed to gain empirical equations for the effect of cracks on these failures.

Our results have shown a good correlation with the "Good Bond Conditions" model for bond stress-slip behaviour as proposed by FIB [2012], with the exception of unconfined splitting failures, which are closer to the "All Other Bond Conditions" model. These models can be used to get a conservative value of slip for a given bond stress.

It is shown that failure of a bar in a splitting failure mode can cause a significant reduction of approximately 47% in the strength of bars on the same crack plane. Bars failing in pull-out appear to have no effect on adjacent bars. Further work could be performed to find whether this relationship can be extended to when two bars on the same crack plane are loaded at the same time. In addition, further work should be done to understand the effect of increasing the distance between the bars and also when the crack does not extend between the two bars.

Eurocode 2 [British Standards Institution, 2010] does not explicitly consider the effect of these cracks along the reinforcement. However, it is shown that the codified bond strength value has a significant factor of safety, and therefore it would appear that some amount of cracking along the reinforcement can occur and the design bond strength still developed with a significant factor of safety. It is thought empirical equations for the effect of cracking on splitting and pull-out failure could be developed and used to give confidence in this assumption. Splitting failure, being more destructive than pull-out, will need a higher factor of safety, and will therefore often control analysis, even though pull-out may be the observed failure mechanism.

References

D. A. Abrams. Tests of bond between concrete and steel. *University of Illinois Engineering Experiment Station*, Bulletin No. 71, Dec. 1913.

ACI Committee 318. 318-11: Building Code Requirements for Structural Concrete, 2011.

British Standards Institution. Eurocode 2 : Design of concrete structures, 2010.

J. Cairns and G. Plizzari. Towards a harmonised European bond test. *Materials and Structures*, 36 (October):498–506, 2003.

P. Chana. A test method to establish realistic bond stresses. *Magazine of Concrete Research*, 42(151): 83–90, 1990.

D. Darwin and A. B. Matamoros. ACI Committee Report 408R -Bond and Development of Straight Reinforcing Bars in Tension. Technical report, 2003.

F. M. de Almeida Filho, M. K. El Debs, and A. L. H. C. El Debs. Bond-slip behavior of self-compacting concrete and vibrated concrete using pull-out and beam tests. *Materials and Structures*, 41(6):1073–1089, Oct. 2007. ISSN 1359-5997.

P. Desnerck. *Compressive, Bond and Shear Behaviour of Powder-Type Self-Compacting Concrete*. PhD thesis, Universiteit Gent, 2011.

P. Desnerck, J. M. Lees, and C. T. Morley. Bond Behaviour of Reinforcing Bars in Cracked Concrete, 2015.

R. C. Donahey and D. Darwin. Bond of Top-Cast Bars in Bridge Decks. *ACI Journal*, 82(1):57–66, 1985.

C. Fang, K. Lundgren, L. Chen, and C. Zhu. Corrosion influence on bond in reinforced concrete. *Cement and Concrete Research*, 34(11):2159–2167, Nov. 2004. ISSN 00088846.

Federation Internationale du beton (fib). *Bond of Reinforcement in Concrete : State-of-the-art report*. Lausanne, 2000.

FIB. Model code 2010. Technical report, Lausanne, 2012.

Highways Agency. Interim Advice Note 53/04 - Concrete Half-Joint deck structures, 2004.

P. M. Johnson, A. Couture, and R. Nicolet. Commission of Inquirey into the Collapse of a Portion of the de la Concorde Overpass. Technical report, Commission d'enquete sur le viaduc de la Concorde, Quebec, 2007.

G. Lamé. *Leçons sur la théorie mathématique: de l'élasticité des corps solides*. Bachelier, Paris, 1 edition, 1852.

K. Lundgren. Effect of corrosion on the bond between steel and concrete: an overview. *Magazine of Concrete Research*, 59(6):447–461, Jan. 2007. ISSN 0024-9831.

P. Mangat and M. S. Elgarf. Bond characteristics of corroding reinforcement in concrete beams. *Materials and Structures*, 32:89–97, 1999. ISSN 0025-5432.

RILEM/CEB/FIB. Bond tests for reinforcing steel'. *Matériaux et Constructions*, 3(15):175–178, 1970.

S. Soretz. A comparison of beam tests and pull-out tests. *Matériaux et Construction*, 5(4):261–264, 1972.

T. a. Söylev and R. François. Effects of Bar-Placement Conditions on Steel-Concrete Bond. *Materials and Structures*, 39(2):211–220, Mar. 2006. ISSN 1359-5997.

R. Tepfers. *A Theory of Bond Applied to Overlapped Tensile Reinforcemet Spices for Deformed Bars*. PhD thesis, Chalmers University of Technology, 1973.

G. B. Welch and B. J. F. Patten. Bond Strength of Reinforcement Affected by Concrete Sedimentation. *Journal Of The American Concrete Institute*, 15(62):251–264, 1965.

Part V

Appendices

A Concrete Testing Results

Batch	**For**	**Cast Date**	**Test Date**	f_{cu} **(MPa)**	σ **(MPa)**	f_{ct} **(MPa)**	σ **(MPa)**
Group 1 Casts - November/December 2014							
1	*Series 2 Cylinders*	3/11/14	10/11/14	**21.1**	*0.26*	**2.20**	*0.05*
			12/12/14	**29.6**	*1.1*	**3.10**	*0.35*
2a	*Series 1 (Uncracked) samples*	17/11/14	12/12/14	**31.8**	*3.10*	**3.17**	*0.14*
2b	*Series 2 (Cylinders) filler concrete*		12/12/14	**26.7**	*0.58*	**2.70**	*0.28*
3a	*Series 3a (Tin Foil) & Series 3b (Oil) - top layer*	27/11/14	12/12/14	**23.8**	*0.22*	**2.66**	*0.28*
3b	*Series 3b (Oil) - middle layer*	27/11/14	12/12/14	**27.1**	*1.12*	**2.43**	*0.33*
3c	*Series 3b (Plastic) & Series 3b (Oil) - bottom layer*	27/11/14	12/12/14	**24.0**	*0.51*	**2.39**	*0.23*
Group 2 Casts - February 2015							
4	*Series 6 (Cylinders only) & Series 4 (Uncracked)*	28/1/15	5/2/15	**25.5**	*0.79*	**2.43**	*0.40*
		28/1/15	20/2/15	**29.2**	*0.65*	**3.30**	*0.11*
5	*Series 5 (Plastic)*	28/1/15	20/2/15	**32.8**	*2.45*	**3.11**	*0.13*
6	*Series 6 (Cylinders) - filler concrete*	8/2/15	20/2/15	**30.4**	*0.76*	**2.98**	*0.12*

Figure A.1: Results of Concrete Tests

B Additional Graphs

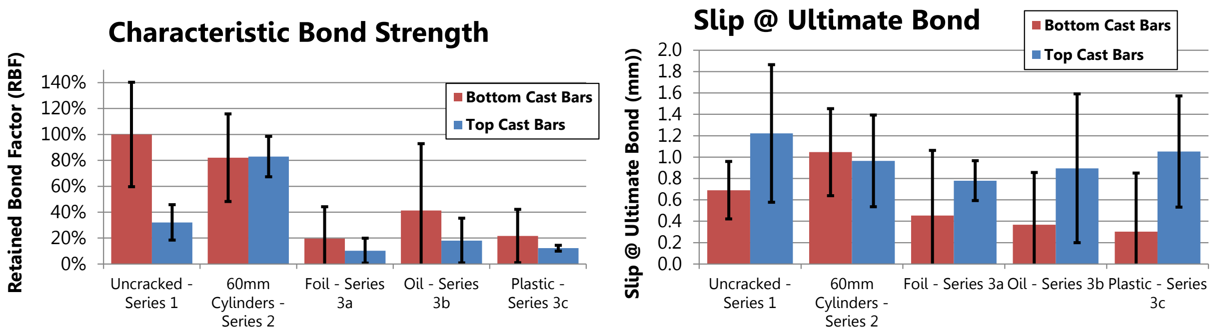

Figure B.1: Additional Graphs - Group 1 Testing

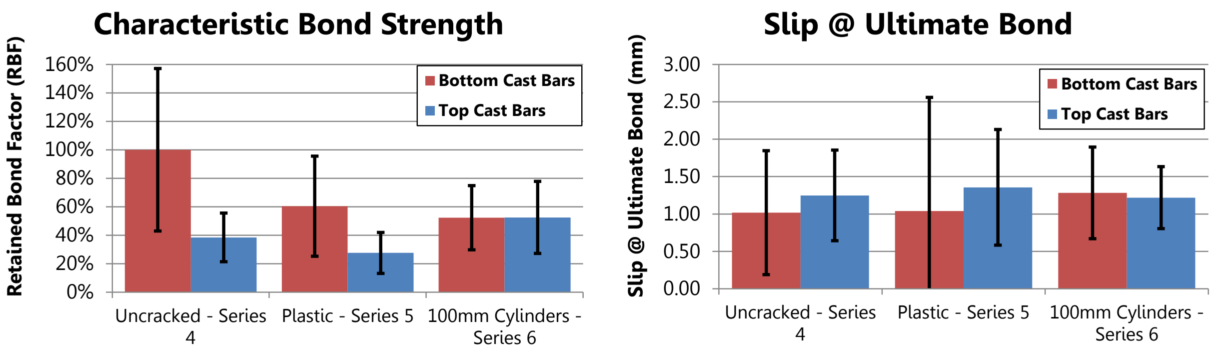

Figure B.2: Additional Graphs - Group 2 Tests

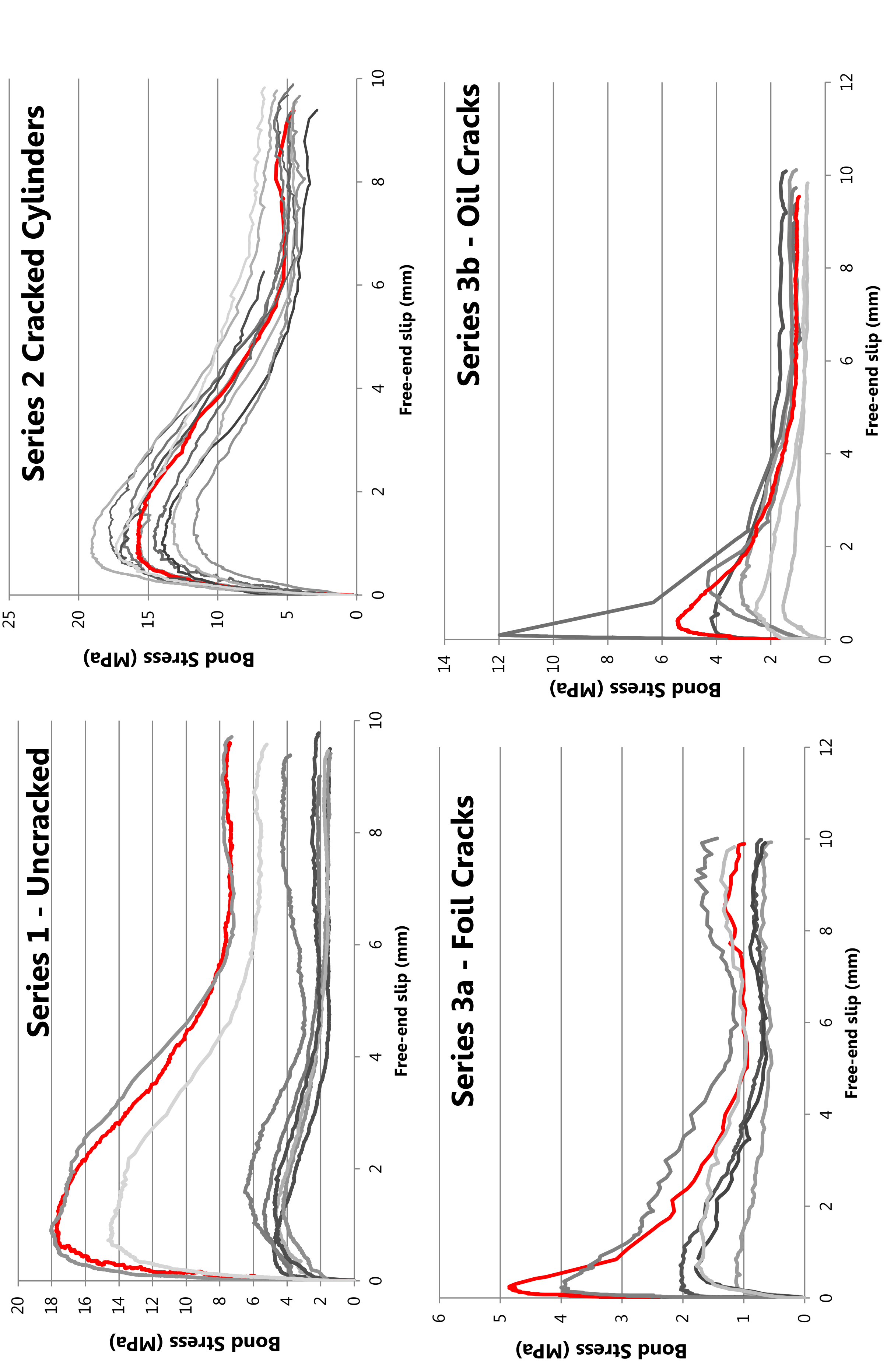

Figure B.3: All result graphs (1 of 2), showing representative curve in red

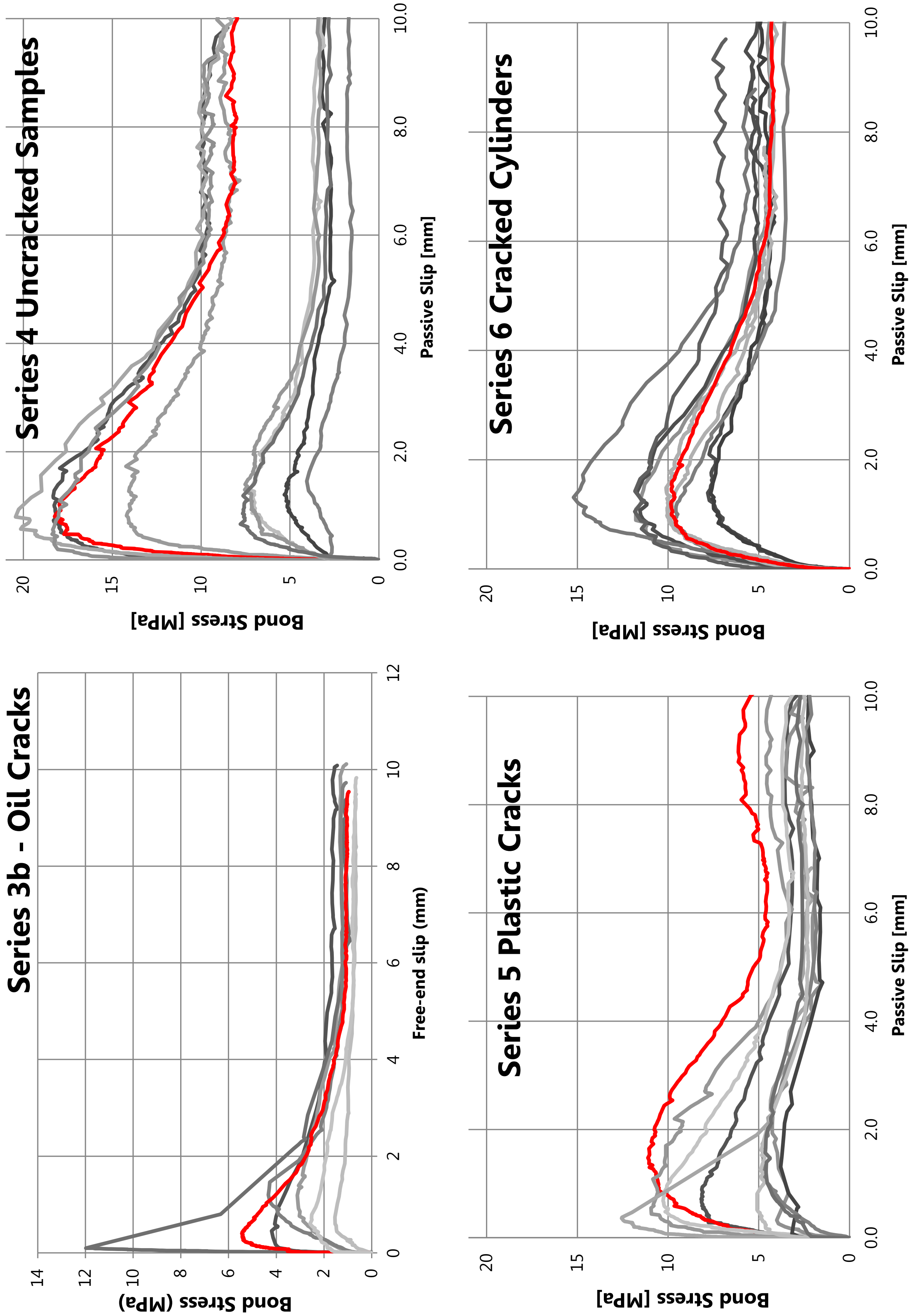

Figure B.4: All result graphs (2 of 2), showing representative curve in red

C Risk Assessment Retrospective

In the course of this project, two full risk assessments were completed and submitted to the Departmental authorities. These covered manufacture and testing of the samples respectively. I (the author) feel that these offered a good assessment of the hazards encountered.

The production of concrete can be dangerous - inhalation of cement dust and concrete coming into contact with skin can cause irritation, which can in some cases be serious. This issue was well understood due to prior experience of using concrete on site, and was emphasised during initial briefings. A Face Fit test was performed on a dust mask - this served the purpose of highlighting the importance of fitting the mask correctly and tightly, which was a problem I had not considered before this test.

Another risk was that of sharp hazards. This had been understood in terms of sanding steel reinforcement and the use of blades, however an unexpected hazard was splinters from the plywood formwork, largely as a result of damage during debonding. It was therefore necessary to repair the formwork, using wood glue and sanding down if necessary, which avoided any incidents as a result of this and showed the importance of remaining vigilant to risks throughout the project.

Were I doing this project again, I would have paid greater attention to designing the test procedure with a view to improve handling, as opposed to simply meeting strength and experimental requirements. The main example of this would have involved making samples smaller to permit one person lifting - the weight of our samples meant handling by one person was limited to shuffling the blocks rather than lifting. Alternatively, I could have included some provision for use of lifting aids, such as lifting hooks. The test setup generally performed well, and, as was predicted in the calculations, suffered no significant deformation - this was expected as very high factors of safety were prescribed due to the use of departmental “meccano”, which was a sensible approach in our laboratory. However if these sections were not available, it would have been necessary to perform more detailed calculations to allow a balance of safety and efficiency (cost). Similar to the previous comment, were I re-designing this rig, I would focus on making it easier to get the sample in place - this required an awkward two person lift to achieve.

Overall, this project included a number of risks. It is therefore felt that the completion of the project without incident was a successful endorsement of this procedure. This project has taught me the importance of both using initial risk assessments to identify issues that perhaps would not have been noted otherwise (for instance, the need to fit a mask well), but also the importance of constantly being alert for risks as they develop and occur.